

---

# Bayesian Model Merging

---

Kaiyang Li<sup>1</sup>   Shaobo Han<sup>2</sup>   Qing Su<sup>1</sup>   Shihao Ji<sup>1</sup>

<sup>1</sup>School of Computing, University of Connecticut, Storrs, CT 06269  
 {kaiyang.li, qing.2.su, shihao.ji}@uconn.edu

<sup>2</sup>Optical Networking and Sensing, NEC Labs America, Princeton, NJ 08540  
 shaobo@nec-labs.com

## Abstract

Model merging aims to combine multiple task-specific expert models into a single model without joint retraining, offering a practical alternative to multi-task learning when data access or computational budget is limited. Existing methods, however, face two key limitations: (1) they overlook the valuable inductive bias of strong anchor models and estimate the merged weights from scratch, and (2) they rely on a shared hyperparameter setting across different modules of the network, lacking a global optimization strategy. This paper introduces **Bayesian Model Merging (BMM)**, a *plug-and-play* bi-level optimization framework, where the inner level formulates the model merging as an activation-based Bayesian regression under a strong prior induced by an anchor model, yielding an efficient closed-form solution; and the outer level leverages a Bayesian optimization procedure to search module-specific hyperparameters globally based on a small validation set. Furthermore, we reveal a key alignment between activation statistics and task vectors, enabling us to derive a data-free variant of BMM that estimates the Gram matrix for regression without any auxiliary data. Across extensive benchmarks, including up to 20-task merging in vision and 5-task merging in language, BMM consistently outperforms all *plug-and-play* anchor baselines (e.g., TA, WUDI-Merging, and TSV). In particular, on the ViT-L/14 benchmark for 8-task merging, a single merged model reaches **95.1**, closely matching the average performance of eight task-specific experts (**95.8**).

## 1 Introduction

Adapting foundation models to downstream tasks via fine-tuning has become standard practice, but maintaining a separate expert model for each task introduces substantial storage, deployment, and operational overhead. While multi-task learning offers a unified alternative [1], it necessitates joint data access and incurs prohibitive computational costs, making it often infeasible under data silos, privacy constraints, or limited computing budgets. Model merging [2–4] offers a practical solution. By directly combining multiple expert models into a single architecture, it enables unified inference without revisiting the original training data or incurring the joint retraining costs. This paradigm has become increasingly relevant with the flourishing ecosystem of open-source models on platforms such as Hugging Face [5], which offers an abundant supply of task-specific experts for integration.

A central challenge in model merging is how to effectively combine expert models when auxiliary data is limited or unavailable. Existing methods fall into two broad regimes based on their use of auxiliary data. *Data-assisted* methods, such as Fisher Merging [2] and RegMean [6], rely on a small calibration set to estimate empirical statistics for merging. *Data-free* methods, including Task Arithmetic (TA) [3], TIES [4], WUDI-Merging [7], TSV [8], and ISO-CTS [9], avoid auxiliary data for estimating merged parameters, though some still use a held-out validation set for lightweight hyperparameter selection. Despite their differences, both regimes suffer from two important limitations. First, they typically estimate merged weights from scratch without exploiting prior knowledge from strong anchor models, leaving valuable inductive bias underused. Second, many advanced methods operate

primarily through module-wise merging in isolation, and adopt a shared hyperparameter setting across different modules for tuning convenience, overlooking module heterogeneity and lacking a global optimization strategy for hyperparameter search.

To address these limitations, we propose **Bayesian Model Merging (BMM)**, a *plug-and-play* bi-level optimization framework that is built on two key ideas. First, instead of estimating merged weights from scratch, BMM leverages prior knowledge from strong anchor models (e.g., TA [3], RegMean [6], or TSV [8]), leading to an activation-based Bayesian regression with an efficient closed-form solution for module-wise merging. Second, rather than relying on a shared hyperparameter setting across all modules, BMM performs globally coordinated architecture-aware Bayesian optimization to adapt regularization strengths across heterogeneous modules of the network. Moreover, we theoretically and empirically reveal a key alignment between activation statistics and module-level task vectors, enabling us to derive a data-free variant of BMM while preserving the closed-form solution.

Empirically, BMM is effective across both vision and language model merging. Across four backbones from two model families and seven *plug-and-play* anchor models, BMM consistently improves over every anchor in both data-assisted and data-free settings, with relative gains of up to 27% on weaker anchors while still improving the strongest ones. In particular, on the standard ViT-L/14 benchmark, a single merged model reaches **95.1%**, closely matching the average performance of eight task-specific experts (**95.8%**). Extensive ablation studies are conducted to further validate the main components and design choices of BMM.

## 2 Related Work

**Training-free model merging** efficiently combines expert checkpoints without full data access or costly joint retraining. Existing methods generally fall into two broad regimes based on their reliance on auxiliary data: *data-assisted* and *data-free*. *Data-assisted methods* leverage a small calibration set or activation statistics to guide the merge. For example, Fisher Merging [2] performs Fisher-weighted average of task-specific models, while RegMean [6] casts linear-layer merging as regression with a closed-form solution. *Data-free methods* eliminate the need of auxiliary data and rely entirely on the weights of the expert models. In this regime, Task Arithmetic (TA) [3] serves as the seminal baseline. Subsequent works mainly mitigate interference among models through sparsification, including TIES [4], DARE [10], PCB-Merging [11], and Localize-and-Stitch [12]. Another line of work (e.g., TSV [8] and ISO-CTS [9]) leverages structured low-rank subspaces to isolate task-specific features or align task-relevant subspaces. More recently, methods such as WUDI-Merging [7] and DOGE [13] optimize explicit data-free merging objectives, but do not exploit prior knowledge from strong anchor models and learn a uniform hyperparameter setting for different modules of the network. Our BMM is complementary to these approaches: it leverages existing merged solutions as anchors, admits an efficient closed-form solution for module-level merging, and exploits bi-level optimization for hyperparameter search across different module groups.

**Representation geometry, neural collapse, and alignment after fine-tuning.** A growing literature investigates the emergence of structured geometry in trained neural networks. Neural collapse [14] shows that during the terminal phase of training, the last-layer features collapse to their class means, and classifier weights align with the same simplex geometry. Neural Feature Ansatz [15] and Deep RFM [16] broaden this perspective to network-wise feature learning and connect the layer-wise weight structure to the average gradient outer products. A recent analysis by Liu et al. [17] further shows that latent representations, network weights, and gradients become mutually aligned across hidden layers. Several recent works [18–20] also connect neural collapse to transfer learning and fine-tuning, including collapse-inspired fine-tuning, transferability estimation, and analyses of downstream geometric complexity, but these studies mainly focus on last-layer collapse, transferability, or downstream fine-tuning behavior. In contrast, we study model merging from task-specific checkpoints, each of which is fine-tuned on a specific downstream task until convergence. We establish a module-wise alignment relation between the Gram matrix of the task vectors and the corresponding second-moment statistics of the activations, and leverage it to derive a data-free variant of BMM with a closed-form solution.

### 3 Problem Definition

**Notation.** Let  $\theta_{\text{pre}} \in \mathbb{R}^d$  denote the parameters of a pretrained base model, and  $\{\theta^{(t)}\}_{t=1}^T$  represent the parameters of  $T$  distinct models fine-tuned from  $\theta_{\text{pre}}$  on different downstream tasks. All models share the same architecture and operate within the same parameter space  $\mathbb{R}^d$ .

**Task Vectors.** Following the framework of Task Arithmetic (TA) [3], we use task vectors to represent task-specific parameter offsets. Specifically, the task vector for the  $t$ -th model is defined as  $\tau^{(t)} = \theta^{(t)} - \theta_{\text{pre}}$ , for  $t \in \{1, \dots, T\}$ .

**Objective.** Given a pretrained model  $\theta_{\text{pre}}$  and task vectors  $\{\tau^{(t)}\}_{t=1}^T$ , our goal is to design an aggregation strategy  $\mathcal{A}$  that combines  $T$  task vectors into a single merged model, parameterized by:

$$\theta_{\text{merged}} = \theta_{\text{pre}} + \mathcal{A}(\tau^{(1)}, \dots, \tau^{(T)}), \quad (1)$$

such that the merged model preserves the task-specific capabilities of all the fine-tuned models as much as possible. We consider model merging without access to the original task-specific training data, and thus multi-task learning isn't applicable. Instead, we study two standard model merging settings: (i) data-assisted, where a small *unlabeled* calibration set is available to guide the merge, and (ii) data-free, where the merging procedure itself uses no auxiliary data. Following the seminal work of TA [3], the data-free merging implies no auxiliary data is used to estimate activation statistics, while a small validation set is still used strictly for hyperparameter tuning.

## 4 Methodology

### 4.1 Model Merging as Bayesian Linear Regression

**Module-wise Decomposition.** While Eq. (1) defines the merging objective at the full parameter space  $\mathbb{R}^d$ , deep neural networks are practically composed of multiple distinct modules (e.g., linear projections in self-attention or MLP blocks). For computational tractability, we decompose the full parameter space  $\mathbb{R}^d$  into module-wise parameter partitions, indexed by  $m = \{1, \dots, M\}$ . Following the approach of WUDI-Merging [7], our aggregation strategy focuses specifically on 2D weight matrices, while keeping all the weights for biases intact. In the following, we will present our merging method at the module level, and the same method applies to all  $M$  modules of the network equally.

Let  $\mathbf{W}_{\text{pre}} \in \mathbb{R}^{d_{\text{out}} \times d_{\text{in}}}$  be one of the  $M$  pretrained 2D weight matrices. We define its module-wise task vector for the  $t$ -th task as the parameter offset  $\mathbf{U}^{(t)} = \mathbf{W}^{(t)} - \mathbf{W}_{\text{pre}}$ . Our core objective is to aggregate these task-specific updates  $\{\mathbf{U}^{(t)}\}_{t=1}^T$  into a single merged task vector  $\mathbf{U}$ , such that the final merged module is parameterized by

$$\mathbf{W}_{\text{merged}} = \mathbf{W}_{\text{pre}} + s \cdot \mathbf{U}, \quad (2)$$

where  $s$  is a scaling hyperparameter that is tuned on a validation set.

**Activation-based Regression.** We frame the estimation of the merged module-wise task vector  $\mathbf{U}$  as an activation-based regression problem. In the data-assisted setting, we collect  $N$  representative activations for the  $t$ -th task, denoted as  $\{\mathbf{x}_n^{(t)}\}_{n=1}^N$ , where  $\mathbf{x}_n^{(t)} \in \mathbb{R}^{d_{\text{in}}}$ . They are collected by passing the task-specific unlabeled calibration data through the corresponding fine-tuned model. To preserve the task-specific capabilities, we aim to align the residual output induced by the merged task vector  $\mathbf{U}$  with that induced by the original task-specific task vectors  $\{\mathbf{U}^{(t)}\}_{t=1}^T$ . Specifically, we define the residual output as  $\mathbf{y}_n^{(t)} = \mathbf{U}^{(t)} \mathbf{x}_n^{(t)} = (\mathbf{W}^{(t)} - \mathbf{W}_{\text{pre}}) \mathbf{x}_n^{(t)}$ . We concatenate all activation vectors column-wise across all  $T$  tasks to construct the activation matrix  $\mathbf{X}$ , and similarly construct the residual output matrix  $\mathbf{Y}$ :

$$\mathbf{X} = [\mathbf{x}_1^{(1)}, \dots, \mathbf{x}_N^{(1)}, \dots, \mathbf{x}_1^{(T)}, \dots, \mathbf{x}_N^{(T)}], \quad \mathbf{Y} = [\mathbf{y}_1^{(1)}, \dots, \mathbf{y}_N^{(1)}, \dots, \mathbf{y}_1^{(T)}, \dots, \mathbf{y}_N^{(T)}]. \quad (3)$$

We assume a linear observation model where the residual outputs  $\mathbf{Y}$  are generated by the merged module-wise task vector  $\mathbf{U}$  acting on  $\mathbf{X}$ , corrupted by Gaussian noise  $\mathbf{E}$ :

$$\mathbf{Y} = \mathbf{UX} + \mathbf{E}, \quad (4)$$

where the noise matrix satisfies  $\mathbf{E}_{:,j} \sim \mathcal{N}(0, \beta^{-1} \mathbf{I})$  independently for each column index  $j$ . Under this linear observation model, the likelihood function of observing  $\mathbf{Y}$  given  $\mathbf{U}$  can be expressed as:

$$p(\mathbf{Y} | \mathbf{U}, \mathbf{X}, \beta) \propto \exp\left(-\frac{\beta}{2} \|\mathbf{Y} - \mathbf{UX}\|_F^2\right). \quad (5)$$

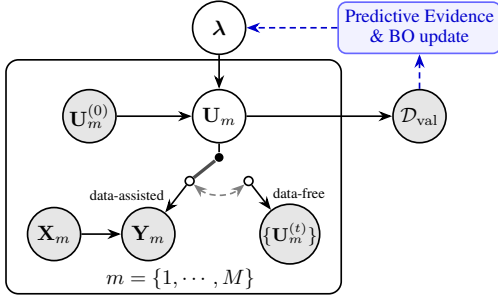


Figure 1: **Probabilistic formulation of BMM.** The framework can adopt different observation sources: empirical activations (data-assisted) or expert weight-induced surrogates (data-free). The inner MAP estimate is solved in closed-form, while the outer loop optimizes  $\lambda$  by BO.

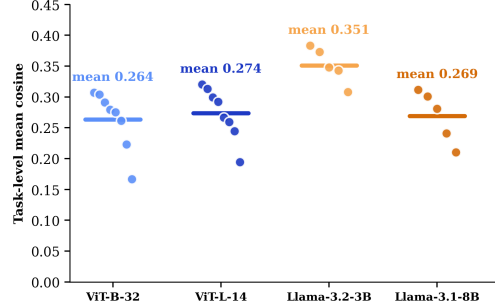


Figure 2: **Alignment between activation statistics and task-vectors** by empirical verification of Theorem 1. The consistent positive cosine similarity scores across vision and language backbones corroborates the proposed alignment between activation statistics and task-vectors.

**Regularization by Anchors.** Purely data-driven estimation of  $\mathbf{U}$  on limited calibration data is not only prone to overfitting but also leaves valuable inductive bias of anchor models (e.g., existing merging solutions) unused. To regularize the solution and inject such priors, we introduce a module-wise *anchor* task vector, defined as  $\mathbf{U}^{(0)} = \mathbf{W}_{\text{anchor}} - \mathbf{W}_{\text{pre}}$ , where  $\mathbf{W}_{\text{anchor}}$  denotes the module weights obtained from an existing merging solution (e.g., TA [3], TIES [4], or TSV [8]). We then impose an element-wise independent Gaussian prior on  $\mathbf{U}$  centered at anchor task vector  $\mathbf{U}^{(0)}$ :

$$p(\mathbf{U}|\mathbf{U}^{(0)}, \alpha) \propto \exp\left(-\frac{\alpha}{2}\|\mathbf{U} - \mathbf{U}^{(0)}\|_F^2\right), \quad (6)$$

where  $\alpha$  controls the precision of this anchor-induced prior. Given these formulations, the *maximum a posteriori* (MAP) estimate of  $\mathbf{U}$  is obtained by maximizing the posterior  $p(\mathbf{U}|\mathbf{Y}, \mathbf{X}) \propto p(\mathbf{Y}|\mathbf{U}, \mathbf{X}, \beta)p(\mathbf{U}|\mathbf{U}^{(0)}, \alpha)$ . Taking the negative logarithm transforms posterior maximization into a minimization problem. Let the regularization weight  $\lambda = \frac{\alpha}{\beta} \geq 0$ , the MAP objective simplifies to:

$$\mathbf{U}_{\text{MAP}} = \arg \min_{\mathbf{U}} \left( \|\mathbf{Y} - \mathbf{U}\mathbf{X}\|_F^2 + \lambda \|\mathbf{U} - \mathbf{U}^{(0)}\|_F^2 \right), \quad (7)$$

where  $\lambda$  balances the empirical fit on the task-specific activations (the first term) with the prior knowledge encapsulated by the anchor model (the second term). Let the derivative of the objective above w.r.t.  $\mathbf{U}$  to be zero, we derive a closed-form solution for the optimal module-wise task vector:

$$\mathbf{U}_{\text{MAP}} = \left( \mathbf{Y}\mathbf{X}^\top + \lambda\mathbf{U}^{(0)} \right) \left( \mathbf{X}\mathbf{X}^\top + \lambda\mathbf{I} \right)^{-1}, \quad (8)$$

where  $\mathbf{I} \in \mathbb{R}^{d_{\text{in}} \times d_{\text{in}}}$  is the identity matrix. Given a  $\lambda \geq 0$ , this closed-form solution allows us to compute the optimal merged task vectors for all  $M$  modules efficiently<sup>1</sup>.

## 4.2 From Predictive Evidence to Bayesian Optimization

Eq. (8) treats all  $M$  modules of the network in isolation for module-wise linear regression. As neural network modules are highly coupled, we need jointly coordinate module-wise regularization strengths (i.e.,  $\lambda$ 's) to maximize the end-to-end performance of the full network. We cast this global coordination as a Bayesian model selection problem. Specifically, we evaluate the predictive evidence of merged model on a held-out validation set  $\mathcal{D}_{\text{val}}$ <sup>2</sup>, conditioned on the local activation data  $\mathcal{D}_{\text{act}} = \{\mathbf{X}_m, \mathbf{Y}_m\}_{m=1}^M$  for data-assisted merging. In the framework of Bayesian model selection, a natural objective is to find  $\lambda^*$  that maximizes the held-out predictive evidence:

$$\lambda^* = \arg \max_{\lambda \geq 0} p(\mathcal{D}_{\text{val}} | \mathcal{D}_{\text{act}}, \mathcal{U}^{(0)}, \lambda). \quad (9)$$

<sup>1</sup>The MAP point estimate of  $\mathbf{U}$  is used mainly for the purpose of computational efficiency. Note that the covariance of the Gaussian posterior also has a closed-form solution, enabling us to sample from the posterior effectively. The corresponding sampling-based BMM is presented in Appendix B, which demonstrates improved uncertainty calibration.

<sup>2</sup>This is the same validation set used by other merging methods (e.g., TA [3], RegMean [6], and TSV [8]) for hyperparameter selection. Therefore, BMM uses no extra data for model merging and represents a fair comparison.

---

**Algorithm 1** Bayesian Bi-level Optimization for Model Merging
 

---

**Require:** Anchors  $\mathcal{U}^{(0)} = \{\mathbf{U}_m^{(0)}\}_{m=1}^M$ , Activation data  $\{\mathbf{X}_m, \mathbf{Y}_m\}_{m=1}^M$ , Val set  $\mathcal{D}_{\text{val}}$ , #Iters  $K$   
**Ensure:** Merged module-wise task vectors  $\mathcal{U}^*$

- 1: Initialize evaluation history  $\mathcal{H} \leftarrow \emptyset$  and  $\mathcal{GP}$  surrogate  $\mathcal{M}$
- 2: **for**  $k = 1, 2, \dots, K$  **do**
- 3:   *# Outer Loop: Surrogate-Guided Proposal*
- 4:    $\boldsymbol{\lambda}^{(k)} \leftarrow \arg \max_{\boldsymbol{\lambda}} \text{EI}(\boldsymbol{\lambda}; \mathcal{M})$   $\triangleright$  Maximize acquisition function
- 5:   *# Inner Loop: Closed-form MAP solution*
- 6:   **for each** module  $m \in \{1, \dots, M\}$  **do**
- 7:      $\mathbf{U}_m^* \leftarrow \left( \mathbf{Y}_m \mathbf{X}_m^\top + \lambda_m^{(k)} \mathbf{U}_m^{(0)} \right) \left( \mathbf{X}_m \mathbf{X}_m^\top + \lambda_m^{(k)} \mathbf{I} \right)^{-1}$   $\triangleright$  Solve inner MAP via Eq. (8)
- 8:   **end for**
- 9:   Assemble full merged model  $\mathcal{U}_{(k)}^* \leftarrow \{\mathbf{U}_m^*\}_{m=1}^M$
- 10:   *# Outer Loop: Validation evaluation*
- 11:    $f^{(k)} \leftarrow \text{Score}(\mathcal{U}_{(k)}^*, \mathcal{D}_{\text{val}})$
- 12:    $\mathcal{H} \leftarrow \mathcal{H} \cup \{(\boldsymbol{\lambda}^{(k)}, f^{(k)})\}$ ; Update surrogate  $\mathcal{M}$
- 13: **end for**
- 14:  $\boldsymbol{\lambda}^* \leftarrow \arg \max_{(\boldsymbol{\lambda}, f) \in \mathcal{H}} f$   $\triangleright$  Extract global optimal configuration
- 15: **return**  $\mathcal{U}^*(\boldsymbol{\lambda}^*)$

---

Let  $\mathcal{U} = \{\mathbf{U}_m\}_{m=1}^M$  be latent variables, the predictive evidence can be expressed as

$$p(\mathcal{D}_{\text{val}} | \mathcal{D}_{\text{act}}, \mathcal{U}^{(0)}, \boldsymbol{\lambda}) = \int p(\mathcal{D}_{\text{val}} | \mathcal{U}) p(\mathcal{U} | \mathcal{D}_{\text{act}}, \mathcal{U}^{(0)}, \boldsymbol{\lambda}) d\mathcal{U}. \quad (10)$$

Eqs. (9) and (10) formalizes a global optimization strategy: the optimal  $\boldsymbol{\lambda}^*$  is determined by maximizing the predictive evidence, effectively accounting for the uncertainty of latent task vectors  $\mathcal{U}$  through marginalization.

To reconcile this Bayesian model selection with practical constraints, we introduce two key refinements. First, to align the objective with the downstream task performances, we replace the intractable likelihood  $p(\mathcal{D}_{\text{val}} | \mathcal{U})$  with a validation utility  $\text{Score}(\cdot)$ , which is the average accuracy of merged model on validation sets across  $T$  tasks:

$$p(\mathcal{D}_{\text{val}} | \mathcal{U}) \propto \text{Score}(\mathcal{U}, \mathcal{D}_{\text{val}}) = \frac{1}{T} \sum_{t=1}^T \text{Acc}_t(\theta_{\text{merged}}(\mathcal{U}), \mathcal{D}_{\text{val}}^{(t)}), \quad (11)$$

where  $\theta_{\text{merged}}(\mathcal{U})$  reconstructs the weights of merged model via Eq. (2). Second, we adopt an empirical-Bayes approximation to bypass the integration in Eq. (10), which is in general prohibitive for deep networks. Specifically, by substituting the full posterior  $p(\mathcal{U} | \mathcal{D}_{\text{act}}, \mathcal{U}^{(0)}, \boldsymbol{\lambda})$  with a point estimate  $\mathcal{U}^*(\boldsymbol{\lambda})$ , we transform the marginalization into a bi-level optimization problem:

$$\boldsymbol{\lambda}^* = \arg \max_{\boldsymbol{\lambda} \geq \mathbf{0}} \text{Score}(\mathcal{U}^*(\boldsymbol{\lambda}), \mathcal{D}_{\text{val}}), \quad (12)$$

subject to

$$\mathcal{U}^*(\boldsymbol{\lambda}) = \arg \max_{\mathcal{U}} p(\mathcal{U} | \mathcal{D}_{\text{act}}, \mathcal{U}^{(0)}, \boldsymbol{\lambda}). \quad (13)$$

The inner optimization in Eq. (13) admits a closed-form solution via Eq. (8). Therefore, the remaining task is to optimize the outer objective in Eq. (12). We treat this outer objective as a black-box function of  $\boldsymbol{\lambda}$ , where each evaluation requires reconstructing a full merged model and measuring its validation performance. For optimization efficiency, we adopt a Gaussian process ( $\mathcal{GP}$ )-based Bayesian Optimization (BO) [21]. At iteration  $k$ , given the evaluation history  $\mathcal{H}_{k-1} = \{(\boldsymbol{\lambda}^{(i)}, f^{(i)})\}_{i=1}^{k-1}$ , where  $f^{(i)} = \text{Score}(\mathcal{U}^*(\boldsymbol{\lambda}^{(i)}), \mathcal{D}_{\text{val}})$ , we fit a  $\mathcal{GP}$  surrogate over  $\boldsymbol{\lambda}$ . We then select the next candidate  $\boldsymbol{\lambda}^{(k)}$  by maximizing an acquisition function, e.g., Expected Improvement (EI), which balances exploitation (high predicted utility) and exploration (high uncertainty). For the selected candidate  $\boldsymbol{\lambda}^{(k)}$ , we solve the corresponding inner MAP problem, evaluate its validation score  $f^{(k)}$ , and update the evaluation history to  $\mathcal{H}_k$ . The best configuration observed during the search is returned as  $\boldsymbol{\lambda}^*$ . This Bayesian bi-level optimization procedure is summarized in Algorithm 1.

The naïve decomposition of full model parameters into  $M$  independent weight matrices poses a severe computational bottleneck for  $\mathcal{GP}$ -based BO (e.g.,  $M = 96$  for ViT-L/14 and  $M = 196$  for

Llama-3.1-8B). To reconcile search efficiency with architectural expressiveness, we propose a block-wise parameter tying strategy. Specifically, we partition the network’s consecutive Transformer layers into  $B$  sequential blocks. Within each block, modules sharing identical functional roles are tied into four module groups: attention-in (Q/K/V), attention-out, MLP-in, and MLP-out. Combined with a block-specific scaling factor  $s$  (Eq. 2), this reduces the parameterization to a compact 5-dimensional search subspace per block, yielding a total BO search space of  $5B$  dimensions. This architecture-aware module decomposition ensures that the merging run-time of BMM remains competitive with state-of-the-art methods, such as TSV [8], WUDI-Merging [7], and ISO-CTS [9].

### 4.3 From Data-Assisted to Data-Free

The MAP estimate of  $\mathbf{U}$  in Eq. (8) performs effectively in the data-assisted setting, where a small unlabeled calibration set is available to assess  $\mathbf{X}$  and  $\mathbf{Y}$  for merging. However, in many practical scenarios, such a calibration set is often unavailable due to privacy or storage constraints. To support this data-free setting, we investigate and reveal a key alignment between activation statistics and task vectors based on recent work of representation geometry and neural collapse [14, 17, 18], which allows us to derive a data-free variant of BMM. In the following, we will present our analysis at the module level, and the same analysis applies to all  $M$  modules of the network equally.

**Alignment between Activation Statistics and Task Vectors.** Let  $\mathbf{x}$  denote an input activation to module  $\mathbf{W}^{(t)}$  and  $\mathbf{y} = \mathbf{U}^{(t)}\mathbf{x} = (\mathbf{W}^{(t)} - \mathbf{W}_{\text{pre}})\mathbf{x}$  the corresponding residual output. Under a set of mild assumptions, the following theorem holds, with the proof provided in Appendix A.

**Theorem 1.** *Under Assumption 1, the Gram matrix of input activations and the Gram matrix of task-vectors have a positively correlated alignment:*

$$\cos_F\left(\mathbb{E}[\mathbf{x}\mathbf{x}^\top], (\mathbf{U}^{(t)})^\top \mathbf{U}^{(t)}\right) > \alpha_t, \quad (14)$$

where  $\alpha_t \in (0, 1]$  is the alignment constant in Assumption 1, and  $\cos_F(\mathbf{A}, \mathbf{B}) = \text{Tr}(\mathbf{A}^\top \mathbf{B}) / (\|\mathbf{A}\|_F \|\mathbf{B}\|_F)$  is the Frobenius cosine-similarity.

To empirically validate Theorem 1, we first estimate  $\mathbb{E}[\mathbf{x}\mathbf{x}^\top]$  by its empirical mean,  $\mathbb{E}[\mathbf{x}\mathbf{x}^\top] \approx \frac{1}{N} \mathbf{X}^{(t)} (\mathbf{X}^{(t)})^\top$ , where  $\mathbf{X}^{(t)} = [\mathbf{x}_1^{(t)}, \dots, \mathbf{x}_N^{(t)}]$  is collected the same as in Eq. 3 from  $N$  calibration samples. We quantify the correlation between  $\mathbf{A} = \frac{1}{N} \mathbf{X}^{(t)} (\mathbf{X}^{(t)})^\top$  and  $\mathbf{B} = (\mathbf{U}^{(t)})^\top \mathbf{U}^{(t)}$  by using the Frobenius cosine-similarity:  $\cos_F(\mathbf{A}, \mathbf{B})$ . Figure 2 reports the task-level cosine similarity scores and its means on the 8-task vision and 5-task language benchmarks across four different backbone architectures. The positive correlation scores ( $>0.26$ ) consistently across four benchmarks empirically corroborate our theoretical analysis.

**Data-Free MAP Estimate of  $\mathbf{U}$ .** According to Theorem 1, we further approximate  $\mathbf{X}^{(t)} (\mathbf{X}^{(t)})^\top \approx c(\mathbf{U}^{(t)})^\top \mathbf{U}^{(t)}$ , where  $c > 0$  is a positive scalar thanks to the positive correlation between activation statistics and task vectors. Along with the forward relation  $\mathbf{Y}^{(t)} = \mathbf{U}^{(t)} \mathbf{X}^{(t)}$ , we can derive a data-free MAP estimate of  $\mathbf{U}$  by inserting them into Eq. (8), which yields:

$$\mathbf{U}_{\text{MAP}}^*(\tilde{\lambda}) = \left( \sum_{t=1}^T \mathbf{U}^{(t)} (\mathbf{U}^{(t)})^\top \mathbf{U}^{(t)} + \tilde{\lambda} \mathbf{U}^{(0)} \right) \left( \sum_{t=1}^T (\mathbf{U}^{(t)})^\top \mathbf{U}^{(t)} + \tilde{\lambda} \mathbf{I} \right)^{-1}, \quad (15)$$

with  $\tilde{\lambda} = \lambda/c$ . This estimate bypasses the need of a calibration set to assess the local activation data  $\{\mathbf{X}, \mathbf{Y}\}$  for model merging, and the merged task vector  $\mathbf{U}$  depends merely on the task-specific task vectors  $\{\mathbf{U}^{(t)}\}_{t=1}^T$ . Similarly,  $\tilde{\lambda}$  can be included in  $\lambda$  and tuned by BO as shown in Algorithm 1.

## 5 Experiments

We evaluate BMM for both vision tasks and language tasks across four backbone architectures with seven different anchor models, which are also the baseline models for performance comparison. Ablation studies are conducted to further validate the main components and design choices of BMM. All our experiments are conducted on a server equipped with 8 NVIDIA RTX-6000 48GB GPUs.

Table 1: Model merging on vision tasks with ViT architectures. The blue subscript values indicate the **relative percentage improvement** compared to the corresponding *anchor*. (Indiv.: Individual)

Model	Tasks	Setting	Indiv.	Pretrained	TA	TIES	RegMean	TSV	WUDI	ISO-CTS
ViT-B/32	8	anchor	92.8	47.7	70.4	75.7	82.3	85.9	<b>87.0</b>	86.4
		data-assisted	-	84.8 <sub>+77.8</sub>	85.0 <sub>+20.7</sub>	85.7 <sub>+13.1</sub>	85.2 <sub>+3.5</sub>	88.9 <sub>+3.5</sub>	89.4 <sub>+2.8</sub>	<b>90.2</b> <sub>+4.3</sub>
		data-free	-	87.9 <sub>+84.4</sub>	87.0 <sub>+23.6</sub>	87.0 <sub>+14.9</sub>	87.9 <sub>+6.8</sub>	87.8 <sub>+2.2</sub>	87.6 <sub>+0.7</sub>	<b>89.0</b> <sub>+3.0</sub>
	14	anchor	90.9	56.9	65.2	68.2	76.6	79.9	80.5	<b>81.5</b>
		data-assisted	-	78.9 <sub>+38.8</sub>	79.2 <sub>+21.5</sub>	79.7 <sub>+16.8</sub>	79.1 <sub>+3.2</sub>	84.3 <sub>+5.5</sub>	84.6 <sub>+5.1</sub>	<b>85.5</b> <sub>+4.9</sub>
		data-free	-	82.7 <sub>+45.4</sub>	82.4 <sub>+26.4</sub>	82.3 <sub>+20.6</sub>	82.9 <sub>+8.2</sub>	82.8 <sub>+3.7</sub>	81.7 <sub>+1.5</sub>	<b>84.3</b> <sub>+3.5</sub>
	20	anchor	91.3	55.7	60.4	64.0	72.2	76.9	76.1	<b>77.6</b>
		data-assisted	-	75.6 <sub>+35.7</sub>	75.5 <sub>+25.0</sub>	76.3 <sub>+19.2</sub>	75.9 <sub>+5.0</sub>	82.0 <sub>+6.7</sub>	82.2 <sub>+8.0</sub>	<b>82.8</b> <sub>+6.6</sub>
		data-free	-	80.0 <sub>+43.5</sub>	78.4 <sub>+29.8</sub>	79.2 <sub>+23.7</sub>	79.7 <sub>+10.4</sub>	79.7 <sub>+3.7</sub>	78.0 <sub>+2.6</sub>	<b>81.5</b> <sub>+5.0</sub>
ViT-L/14	8	anchor	95.8	65.1	84.8	87.0	90.0	93.0	94.0	<b>94.8</b>
		data-assisted	-	92.3 <sub>+41.7</sub>	92.8 <sub>+9.4</sub>	93.1 <sub>+7.1</sub>	92.7 <sub>+2.9</sub>	94.4 <sub>+1.6</sub>	94.7 <sub>+0.7</sub>	<b>95.1</b> <sub>+0.3</sub>
		data-free	-	94.4 <sub>+44.9</sub>	94.2 <sub>+11.0</sub>	94.2 <sub>+8.3</sub>	94.0 <sub>+4.5</sub>	94.4 <sub>+1.5</sub>	94.3 <sub>+0.3</sub>	<b>95.0</b> <sub>+0.2</sub>
	14	anchor	94.3	68.5	79.4	80.2	85.5	89.1	90.5	<b>91.0</b>
		data-assisted	-	88.0 <sub>+28.5</sub>	88.3 <sub>+11.2</sub>	88.3 <sub>+10.1</sub>	88.2 <sub>+3.2</sub>	91.6 <sub>+2.7</sub>	91.7 <sub>+1.3</sub>	<b>92.2</b> <sub>+1.4</sub>
		data-free	-	90.9 <sub>+32.8</sub>	90.9 <sub>+14.5</sub>	90.8 <sub>+13.3</sub>	90.6 <sub>+6.0</sub>	91.3 <sub>+2.4</sub>	91.0 <sub>+0.5</sub>	<b>92.1</b> <sub>+1.2</sub>
	20	anchor	94.7	65.4	74.0	76.7	82.8	87.7	88.4	<b>90.1</b>
		data-assisted	-	86.0 <sub>+31.5</sub>	86.2 <sub>+16.5</sub>	86.4 <sub>+12.6</sub>	86.2 <sub>+4.1</sub>	90.9 <sub>+3.6</sub>	90.8 <sub>+2.7</sub>	<b>91.5</b> <sub>+1.5</sub>
		data-free	-	89.8 <sub>+37.3</sub>	89.6 <sub>+21.1</sub>	89.5 <sub>+16.6</sub>	89.4 <sub>+7.9</sub>	90.3 <sub>+3.0</sub>	89.7 <sub>+1.5</sub>	<b>91.1</b> <sub>+1.1</sub>
<b>Avg. Improvement</b>	data-assisted	-	+42.3	+17.4	+13.1	+3.7	+3.9	+3.4	+3.2	
	data-free	-	+48.0	+21.1	+16.2	+7.3	+2.7	+1.2	+2.3	

## 5.1 Experimental Settings

**Datasets and Models.** For *vision* tasks, we follow the scalability evaluation settings of [8, 9], covering 8-, 14-, and 20-task merging scenarios with ViT-B/32 and ViT-L/14 backbones. For *language* tasks, following [22], we evaluate BMM for 5-task merging based on Llama-3.2-3B and Llama-3.1-8B. To avoid data leakage, we keep the training, validation, and test splits disjoint across tasks. Validation data are used only for hyperparameter search, and test data are used exclusively for final evaluation. Full benchmark descriptions, metrics, and asset/license info are provided in Appendix C.

**Baselines.** For performance comparison, we choose six model merging methods, including Reg-Mean [6], a data-assisted method that relies on an unlabeled calibration set to guide the merging, and five data-free merging methods: TA [3], TIES [4], TSV [8], WUDI-Merging [7], and ISO-CTS [9]. The generated models are also used as the anchors that serve as the prior knowledge for BMM. Additionally, we consider an anchor model that is the original pre-trained backbone, such that  $\mathbf{U}^{(0)} = \mathbf{0}$ , indicating no prior knowledge is used for BMM. We compare BMM with all seven aforementioned anchors as well as the individual fine-tuned models for performance comparison.

**Experiment Details.** Following RegMean [6], our data-assisted BMM collects local activation data  $\mathcal{D}_{\text{act}} = \{\mathbf{X}_m, \mathbf{Y}_m\}_{m=1}^M$  using 128 and 1,000 samples per task for ViT and Llama, respectively. We partition the networks into  $B = 3$  (ViT) and  $B = 1$  (Llama) sequential blocks. Each block has 5 hyperparameters to tune: one scale  $s \in [1.0, 1.3]$  (Eq. 2) and four group-wise regularization strengths  $\lambda$ 's (attention-in/out and MLP-in/out). We sample each  $\lambda$  in the log-scale uniformly from  $[10^{-4}, 1]$  for ViT models and  $[10^{-3}, 100]$  for Llama models. With BO budgets of merely  $K = 200$  (ViT) and  $K = 100$  (Llama) trials, optimizing the full 15D/5D spaces requires fewer validation evaluations than a uniform  $15 \times 15$  grid search in 2D space (225 trials), ensuring computational efficiency. Additional complexity analysis and wall-clock runtime breakdowns are provided in Appendix D.

## 5.2 Main Results

**Vision Benchmarks (ViT).** Table 1 reports the performance of BMM on vision tasks with ViT architectures. As can be seen, BMM is an effective *plug-and-play* merging method. Across all evaluated anchors, model capacities, and task scales, BMM yields noticeable improvements in both data-assisted and data-free settings. The gains are especially large over weaker anchors, such as TA and TIES, with average relative improvements of 21.1% and 16.2%, respectively. At the same time, BMM also consistently outperforms strong recent anchors such as WUDI-Merging and ISO-CTS.

Table 2: Model merging on language tasks with Llama architectures. The blue subscript values indicate the **relative percentage improvement** compared to the corresponding *anchor*.

Model	Setting	Indiv.	Pretrained	TA	TIES	RegMean	TSV	WUDI	ISO-CTS
Llama-3.2-3B	anchor	0.499	0.301	0.438	0.435	0.377	<b>0.471</b>	0.461	0.441
	data-assisted	-	0.302 <sub>+0.3</sub>	0.448 <sub>+2.3</sub>	0.447 <sub>+2.8</sub>	0.406 <sub>+7.7</sub>	0.478 <sub>+1.5</sub>	<b>0.479</b> <sub>+3.9</sub>	0.454 <sub>+2.9</sub>
	data-free	-	0.303 <sub>+0.7</sub>	0.455 <sub>+3.9</sub>	0.468 <sub>+7.6</sub>	0.456 <sub>+21.0</sub>	<b>0.486</b> <sub>+3.2</sub>	0.478 <sub>+3.7</sub>	0.457 <sub>+3.6</sub>
Llama-3.1-8B	anchor	0.630	0.385	0.541	0.554	0.526	0.557	<b>0.560</b>	0.556
	data-assisted	-	0.387 <sub>+0.5</sub>	0.568 <sub>+5.0</sub>	<b>0.579</b> <sub>+4.5</sub>	0.530 <sub>+0.8</sub>	0.574 <sub>+3.1</sub>	0.564 <sub>+0.7</sub>	0.576 <sub>+3.6</sub>
	data-free	-	0.387 <sub>+0.5</sub>	0.568 <sub>+5.0</sub>	0.558 <sub>+0.7</sub>	0.528 <sub>+0.4</sub>	<b>0.573</b> <sub>+2.9</sub>	0.561 <sub>+0.2</sub>	0.564 <sub>+1.4</sub>
<b>Avg. Improvement</b>	data-assisted	-	+0.4	+3.6	+3.6	+4.2	+2.3	+2.3	+3.3
	data-free	-	+0.6	+4.4	+4.2	+10.7	+3.0	+1.9	+2.5

Table 3: Different hyperparameter search methods (*shared- $\lambda$* , *random search*, and *BO*) and their impacts on 8-, 14-, and 20-task merging with ViT-B/32 architecture. Results for data-assisted and data-free variants are reported as mean  $\pm$  std over seeds 0–4.

Setting	Variant	8 Tasks			14 Tasks			20 Tasks		
		TSV	WUDI	ISO-CTS	TSV	WUDI	ISO-CTS	TSV	WUDI	ISO-CTS
anchor	-	85.9	87.0	86.4	79.9	80.5	81.5	76.9	76.1	77.6
data-assisted	shared- $\lambda$	88.1 $\pm$ 0.01	89.0 $\pm$ 0.01	89.3 $\pm$ 0.01	83.2 $\pm$ 0.00	83.5 $\pm$ 0.00	83.9 $\pm$ 0.00	80.1 $\pm$ 0.01	80.6 $\pm$ 0.01	80.3 $\pm$ 0.02
	random	88.6 $\pm$ 0.09	89.2 $\pm$ 0.02	89.7 $\pm$ 0.24	83.7 $\pm$ 0.11	83.9 $\pm$ 0.30	84.9 $\pm$ 0.07	80.6 $\pm$ 0.18	81.2 $\pm$ 0.32	81.7 $\pm$ 0.37
	<b>BO</b>	<b>88.9<math>\pm</math>0.05</b>	<b>89.4<math>\pm</math>0.02</b>	<b>90.2<math>\pm</math>0.03</b>	<b>84.3<math>\pm</math>0.04</b>	<b>84.6<math>\pm</math>0.04</b>	<b>85.5<math>\pm</math>0.06</b>	<b>82.0<math>\pm</math>0.04</b>	<b>82.2<math>\pm</math>0.06</b>	<b>82.8<math>\pm</math>0.05</b>
data-free	shared- $\lambda$	87.1 $\pm$ 0.00	87.1 $\pm$ 0.02	88.0 $\pm$ 0.00	81.5 $\pm$ 0.00	80.7 $\pm$ 0.00	82.7 $\pm$ 0.00	77.9 $\pm$ 0.00	76.7 $\pm$ 0.01	78.8 $\pm$ 0.00
	random	87.4 $\pm$ 0.20	87.4 $\pm$ 0.13	88.1 $\pm$ 0.23	82.2 $\pm$ 0.24	81.2 $\pm$ 0.08	83.3 $\pm$ 0.18	79.0 $\pm$ 0.18	77.3 $\pm$ 0.20	80.0 $\pm$ 0.33
	<b>BO</b>	<b>87.8<math>\pm</math>0.04</b>	<b>87.6<math>\pm</math>0.04</b>	<b>89.0<math>\pm</math>0.03</b>	<b>82.8<math>\pm</math>0.03</b>	<b>81.7<math>\pm</math>0.06</b>	<b>84.3<math>\pm</math>0.05</b>	<b>79.7<math>\pm</math>0.05</b>	<b>78.0<math>\pm</math>0.02</b>	<b>81.5<math>\pm</math>0.04</b>

In addition, BMM remains effective as the number of merged tasks increases. For example, in the 20-task setting with ViT-B/32, BMM with ISO-CTS as anchor improves the merging performance from 77.6% to 82.8% in the data-assisted setting and to 81.5% in the data-free setting. Similar gains are also observed on ViT-L/14, suggesting that BMM can effectively alleviate task interference in larger-scale merging settings.

Finally, BMM brings the performance of model merging close to that of individual task-specific experts. On the ViT-L/14 8-task benchmark, BMM with ISO-CTS as anchor achieves 95.1% in the data-assisted setting and 95.0% in the data-free setting, closely matching the average performance (95.8%) of the eight individual fine-tuned models. Detailed experimental results of mean  $\pm$  std over five random seeds and the per-task breakdowns are provided in Appendices E.1 and E.2, respectively.

**Language Benchmarks (Llama).** Similar to the vision benchmarks, Table 2 shows that BMM consistently improves performance across all anchor models on the 5-task language benchmarks. The gains are especially pronounced for weaker anchors, with the largest improvement reaching 21.0% for RegMean on Llama-3.2-3B in the data-free setting. Importantly, BMM also pushes already competitive anchors to stronger results. For instance, in the data-free setting, BMM improves the TSV anchor from 0.471 to 0.486 on Llama-3.2-3B, achieving the best 3B result among all the merging methods. On Llama-3.1-8B, BMM improves the TSV anchor from 0.557 to 0.573, while the data-assisted BMM with TIES reaches the overall best 8B performance of 0.579. Interestingly, the data-free BMM is particularly strong on the 3B model and often outperforms its data-assisted counterpart, suggesting that the proposed alignment-based approximation can generalize effectively even without auxiliary calibration data. Category-level language breakdowns are provided in Appendix E.2.

### 5.3 Ablation Study

**Effectiveness of BO-based global coordination.** To investigate the effectiveness of BO-based global coordination, Table 3 compares BMM (w/ *BO*) against two hyperparameter-tuning baselines: *shared- $\lambda$*  and *random search*. While *shared- $\lambda$*  assigns a single regularization strength  $\lambda$  to all four module groups and optimizes it via an extensive grid search, *random search* relaxes this constraint by allowing module-specific hyperparameters, but tunes them using 200 trials of random search.

As can be seen from Table 3, *shared- $\lambda$*  already yields substantial improvements over the anchor baselines, confirming that the closed-form MAP estimator is the primary source of performance gains. Relaxing the shared constraint to module-specific hyperparameters with *random search* further

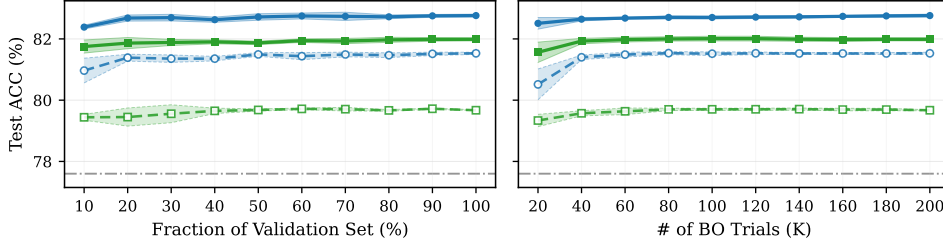


Figure 3: **Ablation study of BMM on 20-task merging (ViT-B/32).** (Left) Test accuracy as a function of the validation set fraction used for Bayesian Optimization (BO). (Right) Test accuracy vs. the number of BO search trials ( $K$ ). All curves report mean  $\pm$  std across 5 seeds. Solid and circle-dashed lines represent data-assisted and data-free BMM. Blue/green colors indicate ISO-CTS/TSV anchors. The horizontal gray dot-dashed line establishes the ISO-CTS baseline.

improves the performance, validating the importance of heterogeneous regularization across different module groups. Finally, BMM (w/ BO) achieves the best overall results by effectively coordinating the module-specific hyperparameters with guided search. Its advantage is most pronounced in the challenging 20-task data-free setting. On the TSV anchor, BMM (w/ BO) reaches an accuracy of 79.7%, compared with 79.0% for *random search* and 77.9% for *shared- $\lambda$*  tuning. This suggests that BO becomes particularly useful when the search space is more complex and the validation signal needs to balance task interference effectively in large-scale merging settings.

**Sensitivity to the Fraction of Validation Set.** Figure 3 (left) reports the final test performance as the fraction of validation set used for BO evolves. Across both TSV and ISO-CTS anchors, and in data-assisted and data-free settings, BMM consistently outperforms the strongest anchor baseline (ISO-CTS) even when a small fraction of the validation set is used. The performance curves are relatively stable from 10% to 100% of the validation set, indicating that the outer-loop optimization is not overly sensitive to the validation-set size. This suggests that BMM can use a small validation subset to reduce the optimization overhead while preserving most of the gains from global hyperparameter search.

**Sensitivity to BO Budget  $K$ .** Figure 3 (right) reports the evolution of final test performance as the number of BO trials ( $K$ ) increases. BMM consistently outperforms the strongest anchor baseline (ISO-CTS) under a small BO budget ( $K$ ). The performance curves reach a plateau after roughly 40 – 60 trials, while increasing the budget further yields only a marginal return. These results indicate that BO is efficient in global hyperparameter search, reaching stable results with a modest budget. Additional runtime-performance comparisons against other methods are reported in Appendix D.3.

## 6 Conclusion

This paper introduces **Bayesian Model Merging (BMM)**, a *plug-and-play* framework for model merging. BMM leverages existing merging solutions as informative priors and formulates module-wise merging as an anchor-regularized Bayesian linear regression with a closed-form solution. To coordinate local merging decisions with end-to-end performance, BMM further adopts a  $\mathcal{GP}$ -based Bayesian optimization to search for regularization strengths globally. We also derive a data-free variant of BMM based on a key alignment between activation statistics and task vectors, while preserving the closed-form solution. Across vision and language benchmarks, BMM consistently improves diverse anchor baselines, scales to challenging 20-task settings, and closely approaches the performance of individual fine-tuned experts on high-capacity ViT architectures. Our results show that combining informative anchors with global hyperparameter coordination provides a practical path towards scalable model merging when auxiliary calibration data is limited or unavailable.

**Limitations and Broader Impacts.** BMM does not exhibit major limitations in the evaluated settings, though our experiments are currently limited to models up to the 8B scale due to computational constraints. Regarding the broader impacts, BMM enables efficient aggregation of task-specific experts without access to original training data, reducing the cost of foundation-model customization. We do not foresee any societal risks beyond those generally associated with large vision and language models, although merged models may inherit biases, safety risks, or domain-specific failures from their underlying experts.

## References

- [1] Sebastian Ruder. An overview of multi-task learning in deep neural networks. *arXiv preprint arXiv:1706.05098*, 2017.
- [2] Michael S. Matena and Colin A. Raffel. Merging models with fisher-weighted averaging. *Advances in Neural Information Processing Systems*, 35:17703–17716, 2022.
- [3] Gabriel Ilharco, Marco Tulio Ribeiro, Mitchell Wortsman, Suchin Gururangan, Ludwig Schmidt, Hannaneh Hajishirzi, and Ali Farhadi. Editing models with task arithmetic. In *The Eleventh International Conference on Learning Representations*, 2023.
- [4] Prateek Yadav, Derek Tam, Leshem Choshen, Colin A. Raffel, and Mohit Bansal. TIES-merging: Resolving interference when merging models. In *Thirty-seventh Conference on Neural Information Processing Systems*, 2023.
- [5] Hugging Face. The hugging face hub. <https://huggingface.co>, 2026. Accessed: 2026-05-04.
- [6] Xisen Jin, Xiang Ren, Daniel Preotiuc-Pietro, and Pengxiang Cheng. Dataless knowledge fusion by merging weights of language models. In *The Eleventh International Conference on Learning Representations*, 2023.
- [7] Runxi Cheng, Feng Xiong, Yongxian Wei, Wanyun Zhu, and Chun Yuan. Whoever started the interference should end it: Guiding data-free model merging via task vectors. In *Proceedings of the 42nd International Conference on Machine Learning*, volume 267 of *Proceedings of Machine Learning Research*, pages 10121–10143. PMLR, 2025.
- [8] Antonio Andrea Gargiulo, Donato Crisostomi, Maria Sofia Bucarelli, Simone Scardapane, Fabrizio Silvestri, and Emanuele Rodolà. Task singular vectors: Reducing task interference in model merging. In *Proceedings of the IEEE/CVF Conference on Computer Vision and Pattern Recognition*, pages 18695–18705, 2025.
- [9] Daniel Marczak, Simone Magistri, Sebastian Cygert, Bartłomiej Twardowski, Andrew D. Bagdanov, and Joost van de Weijer. No task left behind: Isotropic model merging with common and task-specific subspaces. In *Proceedings of the 42nd International Conference on Machine Learning*, volume 267 of *Proceedings of Machine Learning Research*, pages 43177–43199. PMLR, 2025.
- [10] Le Yu, Bowen Yu, Haiyang Yu, Fei Huang, and Yongbin Li. Language models are super mario: Absorbing abilities from homologous models as a free lunch. In *Proceedings of the 41st International Conference on Machine Learning*, volume 235 of *Proceedings of Machine Learning Research*, pages 57755–57775. PMLR, 2024.
- [11] Guodong Du, Junlin Lee, Jing Li, Runhua Jiang, Yifei Guo, Shuyang Yu, Hanting Liu, Sim Kuan Goh, Ho-Kin Tang, Daojing He, and Min Zhang. Parameter competition balancing for model merging. *Advances in Neural Information Processing Systems*, 37, 2024.
- [12] Yifei He, Yuzheng Hu, Yong Lin, Tong Zhang, and Han Zhao. Localize-and-stitch: Efficient model merging via sparse task arithmetic. *Transactions on Machine Learning Research*, 2025. Accepted to TMLR.
- [13] Yongxian Wei, Anke Tang, Li Shen, Zixuan Hu, Chun Yuan, and Xiaochun Cao. Modeling multi-task model merging as adaptive projective gradient descent. In *Proceedings of the 42nd International Conference on Machine Learning*, volume 267 of *Proceedings of Machine Learning Research*, pages 66178–66193. PMLR, 2025.
- [14] Vardan Papyan, X. Y. Han, and David L. Donoho. Prevalence of neural collapse during the terminal phase of deep learning training. *Proceedings of the National Academy of Sciences*, 117(40):24652–24663, 2020.
- [15] Adityanarayanan Radhakrishnan, Daniel Beaglehole, Parthe Pandit, and Mikhail Belkin. Mechanism for feature learning in neural networks and kernel machines. *Science*, 383(6690):1461–1467, 2024.

- [16] Daniel Beaglehole, Peter Súkeník, Marco Mondelli, and Mikhail Belkin. Average gradient outer product as a mechanism for deep neural collapse. In *Advances in Neural Information Processing Systems*, 2024.
- [17] Liu Ziyin, Isaac Chuang, Tomer Galanti, and Tomaso Poggio. Formation of representations in neural networks. In *The Thirteenth International Conference on Learning Representations (ICLR 2025)*, 2025. Spotlight.
- [18] Xiao Li, Sheng Liu, Jinxin Zhou, Xinyu Lu, Carlos Fernandez-Granda, Zhihui Zhu, and Qing Qu. Understanding and improving transfer learning of deep models via neural collapse. *arXiv preprint arXiv:2212.12206*, 2022.
- [19] Yuhe Ding, Bo Jiang, Lijun Sheng, Aihua Zheng, and Jian Liang. Unleashing the power of neural collapse for transferability estimation. *arXiv preprint arXiv:2310.05754*, 2023.
- [20] Michael Munn, Benoit Dherin, and Javier Gonzalvo. The impact of geometric complexity on neural collapse in transfer learning. In *Advances in Neural Information Processing Systems*, 2024.
- [21] Peter I Frazier. Bayesian optimization. In *Recent advances in optimization and modeling of contemporary problems*, pages 255–278. Informa, 2018.
- [22] Yifei He, Siqi Zeng, Yuzheng Hu, Rui Yang, Tong Zhang, and Han Zhao. Mergebench: A benchmark for merging domain-specialized llms. *arXiv preprint arXiv:2505.10833*, 2025.
- [23] Xuhong Li, Yves Grandvalet, and Franck Davoine. Explicit inductive bias for transfer learning with convolutional networks. In *Proceedings of the 35th International Conference on Machine Learning*, pages 2825–2834. PMLR, 2018.
- [24] Zhanxing Zhu, Jingfeng Wu, Bing Yu, Lei Wu, and Jinwen Ma. The anisotropic noise in stochastic gradient descent: Its behavior of escaping from sharp minima and regularization effects. In *Proceedings of the 36th International Conference on Machine Learning*, volume 97 of *Proceedings of Machine Learning Research*, pages 7654–7663. PMLR, 2019.
- [25] Jingfeng Wu, Difan Wang, and Weijie J. Su. The alignment property of SGD noise and how it helps select flat minima: A stability analysis. In *Advances in Neural Information Processing Systems*, volume 35, pages 4680–4693, 2022.
- [26] James Martens and Roger Grosse. Optimizing neural networks with kronecker-factored approximate curvature. In *Proceedings of the 32nd International Conference on Machine Learning*, volume 37 of *Proceedings of Machine Learning Research*, pages 2408–2417. PMLR, 2015.
- [27] Chuan Guo, Geoff Pleiss, Yu Sun, and Kilian Q. Weinberger. On calibration of modern neural networks. In *International Conference on Machine Learning*, 2017.
- [28] Agustinus Kristiadi, Matthias Hein, and Philipp Hennig. Being bayesian, even just a bit, fixes overconfidence in relu networks. In *Proceedings of the 37th International Conference on Machine Learning*, volume 119 of *Proceedings of Machine Learning Research*, pages 5436–5446. PMLR, 2020.
- [29] Jonathan Krause, Michael Stark, Jia Deng, and Li Fei-Fei. 3d object representations for fine-grained categorization. In *ICCV Workshops*, 2013.
- [30] Mircea Cimpoi, Subhransu Maji, Iasonas Kokkinos, Sammy Mohamed, and Andrea Vedaldi. Describing textures in the wild. In *CVPR*, 2014.
- [31] Patrick Helber, Benjamin Bischke, Andreas Dengel, and Damian Borth. Eurosat: A novel dataset and deep learning benchmark for land use and land cover classification. *IEEE Journal of Selected Topics in Applied Earth Observations and Remote Sensing*, 2019.
- [32] Johannes Stallkamp, Marc Schlipsing, Jan Salmen, and Christian Igel. The german traffic sign recognition benchmark: A multi-class classification competition. In *IJCNN*, 2011.
- [33] Yann LeCun, Leon Bottou, Yoshua Bengio, and Patrick Haffner. Gradient-based learning applied to document recognition. *Proceedings of the IEEE*, 1998.

- [34] Gong Cheng, Junwei Han, and Xiaoqiang Lu. Remote sensing image scene classification: Benchmark and state of the art. *Proceedings of the IEEE*, 2017.
- [35] Jianxiong Xiao, James Hays, Krista A. Ehinger, Aude Oliva, and Antonio Torralba. Sun database: Exploring a large collection of scene categories. In *IJCV*, 2016.
- [36] Yuval Netzer, Tao Wang, Adam Coates, Alessandro Bissacco, Bo Wu, and Andrew Y. Ng. Reading digits in natural images with unsupervised feature learning. In *NeurIPS Workshops*, 2011.
- [37] Alex Krizhevsky and Geoffrey Hinton. Learning multiple layers of features from tiny images. Technical report, University of Toronto, 2009.
- [38] Adam Coates, Andrew Ng, and Honglak Lee. An analysis of single-layer networks in unsupervised feature learning. In *AISTATS*, 2011.
- [39] Maria-Elena Nilsback and Andrew Zisserman. Automated flower classification over a large number of classes. In *ICVGIP*, 2008.
- [40] Omkar M. Parkhi, Andrea Vedaldi, Andrew Zisserman, and C. V. Jawahar. Cats and dogs. In *CVPR*, 2012.
- [41] Bastiaan S. Veeling, Jasper Linmans, Jim Winkens, Taco Cohen, and Max Welling. Rotation equivariant cnns for digital pathology. In *MICCAI*, 2018.
- [42] Ian J. Goodfellow, Dumitru Erhan, Pierre Luc Carrier, Aaron Courville, Mehdi Mirza, Ben Hamner, Will Cukierski, Yichuan Tang, David Thaler, Dong-Hyun Lee, et al. Challenges in representation learning: A report on three machine learning contests. *arXiv preprint arXiv:1307.0414*, 2013.
- [43] Gregory Cohen, Saeed Afshar, Jonathan Tapson, and Andre van Schaik. Emnist: Extending mnist to handwritten letters. In *IJCNN*, 2017.
- [44] Lukas Bossard, Matthieu Guillaumin, and Luc Van Gool. Food-101: Mining discriminative components with random forests. In *ECCV*, 2014.
- [45] Han Xiao, Kashif Rasul, and Roland Vollgraf. Fashion-mnist: A novel image dataset for benchmarking machine learning algorithms. *arXiv preprint arXiv:1708.07747*, 2017.
- [46] Richard Socher, Alex Perelygin, Jean Wu, Jason Chuang, Christopher D. Manning, Andrew Y. Ng, and Christopher Potts. Recursive deep models for semantic compositionality over a sentiment treebank. In *EMNLP*, 2013.
- [47] Tarin Clanuwat, Mikel Bober-Irizar, Asanobu Kitamoto, Alex Lamb, Kazuaki Yamamoto, and David Ha. Deep learning for classical japanese literature. *arXiv preprint arXiv:1812.01718*, 2018.
- [48] Nathan Lambert, Jacob Morrison, Valentina Pyatkin, Shengyi Huang, Hamish Ivison, Faeze Brahman, Lester James V Miranda, Alisa Liu, Nouha Dziri, Shane Lyu, et al. Tulu 3: Pushing frontiers in open language model post-training. *arXiv preprint arXiv:2411.15124*, 2024.
- [49] Jeffrey Zhou, Tianjian Lu, Swaroop Mishra, Siddhartha Brahma, Sujoy Basu, Yi Luan, Denny Zhou, and Le Hou. Instruction-following evaluation for large language models. *arXiv preprint arXiv:2311.07911*, 2023.
- [50] Yuxuan Tong, Xiwen Zhang, Rui Wang, Ruidong Wu, and Junxian He. Dart-math: Difficulty-aware rejection tuning for mathematical problem-solving. *Advances in Neural Information Processing Systems*, 37:7821–7846, 2024.
- [51] Jia Li, Edward Beeching, Lewis Tunstall, Ben Lipkin, Roman Soletskyi, Shengyi Huang, Kashif Rasul, Longhui Yu, Albert Q Jiang, Ziju Shen, et al. Numinamath: The largest public dataset in ai4maths with 860k pairs of competition math problems and solutions. Hugging Face repository, 2024.

- [52] Karl Cobbe, Vineet Kosaraju, Mohammad Bavarian, Mark Chen, Heewoo Jun, Lukasz Kaiser, Matthias Plappert, Jerry Tworek, Jacob Hilton, Reiichiro Nakano, et al. Training verifiers to solve math word problems. *arXiv preprint arXiv:2110.14168*, 2021.
- [53] Shivalika Singh, Freddie Vargus, Daniel Dsouza, Börje F Karlsson, Abinaya Mahendiran, Wei-Yin Ko, Herumb Shandilya, Jay Patel, Deividas Mataciunas, Laura OMahony, et al. Aya dataset: An open-access collection for multilingual instruction tuning. *arXiv preprint arXiv:2402.06619*, 2024.
- [54] Viet Lai, Chien Nguyen, Nghia Ngo, Thuat Nguyen, Franck Dernoncourt, Ryan Rossi, and Thien Nguyen. Okapi: Instruction-tuned large language models in multiple languages with reinforcement learning from human feedback. In *Proceedings of the 2023 Conference on Empirical Methods in Natural Language Processing: System Demonstrations*, pages 318–327, 2023.
- [55] Yuxiang Wei, Zhe Wang, Jiawei Liu, Yifeng Ding, and Lingming Zhang. Magicoder: Empowering code generation with oss-instruct. *arXiv preprint arXiv:2312.02120*, 2023.
- [56] Jacob Austin, Augustus Odena, Maxwell Nye, Maarten Bosma, Henryk Michalewski, David Dohan, Ellen Jiang, Carrie Cai, Michael Terry, Quoc Le, et al. Program synthesis with large language models. *arXiv preprint arXiv:2108.07732*, 2021.
- [57] Jiawei Liu, Chunqiu Steven Xia, Yuyao Wang, and Lingming Zhang. Is your code generated by chatGPT really correct? rigorous evaluation of large language models for code generation. In *Thirty-seventh Conference on Neural Information Processing Systems*, 2023.
- [58] Seungju Han, Kavel Rao, Allyson Ettinger, Liwei Jiang, Bill Yuchen Lin, Nathan Lambert, Yejin Choi, and Nouha Dziri. Wildguard: Open one-stop moderation tools for safety risks, jailbreaks, and refusals of llms. *arXiv preprint arXiv:2406.18495*, 2024.
- [59] Liwei Jiang, Kavel Rao, Seungju Han, Allyson Ettinger, Faeze Brahman, Sachin Kumar, Niloofar Mireshghallah, Ximing Lu, Maarten Sap, Yejin Choi, et al. Wildteaming at scale: From in-the-wild jailbreaks to (adversarially) safer language models. *Advances in Neural Information Processing Systems*, 37:47094–47165, 2024.
- [60] Mantas Mazeika, Long Phan, Xuwang Yin, Andy Zou, Zifan Wang, Norman Mu, Elham Sakhaee, Nathaniel Li, Steven Basart, Bo Li, et al. Harmbench: A standardized evaluation framework for automated red teaming and robust refusal. *arXiv preprint arXiv:2402.04249*, 2024.
- [61] Paul Röttger, Hannah Rose Kirk, Bertie Vidgen, Giuseppe Attanasio, Federico Bianchi, and Dirk Hovy. Xstest: A test suite for identifying exaggerated safety behaviours in large language models. *arXiv preprint arXiv:2308.01263*, 2023.
- [62] Gene H. Golub and Charles F. Van Loan. *Matrix Computations*. Johns Hopkins University Press, 4 edition, 2013.
- [63] Carl Edward Rasmussen and Christopher K. I. Williams. *Gaussian Processes for Machine Learning*. MIT Press, 2006.

## A Proof of Theorem 1

Let  $\mathbf{x}$  denote an input activation to module  $\mathbf{W}^{(t)}$  and  $\mathbf{y} = \mathbf{U}^{(t)}\mathbf{x} = (\mathbf{W}^{(t)} - \mathbf{W}_{\text{pre}})\mathbf{x}$  the corresponding residual output. Using standard Stochastic Gradient Descent (SGD) with the  $L_2$  regularization, we define  $\mathbf{g}_y = -\nabla_{\mathbf{y}}\ell$  as the backpropagated descent-direction signal induced by the fine-tune loss  $\ell$ . The single-step parameter update for the task vector  $\mathbf{U}^{(t)}$  is governed by:

$$\delta(\mathbf{U}^{(t)}) = \eta \left( \mathbf{g}_y \mathbf{x}^\top - \rho \mathbf{U}^{(t)} \right), \quad (16)$$

where  $\rho > 0$  is the weight decay coefficient, and  $\eta > 0$  is the learning rate. By defining  $\mathbf{D}^{(t)} = \mathbf{g}_y \mathbf{x}^\top$  as the per-sample descent matrix, we have

$$\delta(\mathbf{U}^{(t)}) = \eta (\mathbf{D}^{(t)} - \rho \mathbf{U}^{(t)}). \quad (17)$$

In order to connect the fine-tuned checkpoints with the *unobserved* activations, we study the activation statistics at the terminal phase of fine-tuning. Since model merging operates on fully fine-tuned checkpoints rather than the intermediate ones, our goal here is not to characterize the full stochastic training trajectory, but to capture the geometric structure of representations from the final converged solutions. Specifically, we assume the fine-tuning process reaches a state that satisfies the following assumption.

**Assumption 1.** *The fine-tuned checkpoint is assumed to converge on task  $t$ , and satisfies the following three conditions:*

1. The expected per-sample descent matrix is aligned with the task vector:  $\mathbb{E}[\mathbf{D}^{(t)}] = \rho \mathbf{U}^{(t)}$ , or equivalently,  $\mathbb{E}[\delta(\mathbf{U}^{(t)})] = \mathbf{0}$ .
2. At convergence, the centered descent matrix fluctuations are assumed to retain a positive Frobenius overlap with the Gram matrix of the mean descent matrix signal. That is, let

$$\bar{\mathbf{D}}^{(t)} = \mathbb{E}[\mathbf{D}^{(t)}], \quad \mathbf{C}_t = \mathbb{E}[(\mathbf{D}^{(t)} - \bar{\mathbf{D}}^{(t)})^\top (\mathbf{D}^{(t)} - \bar{\mathbf{D}}^{(t)})], \quad \mathbf{M}_t = (\bar{\mathbf{D}}^{(t)})^\top \bar{\mathbf{D}}^{(t)}. \quad (18)$$

We have  $\cos_F(\mathbf{C}_t, \mathbf{M}_t) > \alpha_t$ ,  $0 < \alpha_t \leq 1$ , where  $\cos_F(\mathbf{A}, \mathbf{B}) = \text{Tr}(\mathbf{A}^\top \mathbf{B}) / (\|\mathbf{A}\|_F \|\mathbf{B}\|_F)$  is the Frobenius cosine-similarity.

3. The gradient energy factorizes from the second-moment of input activation:

$$\mathbb{E}[\|\mathbf{g}_y\|_2^2 \mathbf{x} \mathbf{x}^\top] = \mathbb{E}[\|\mathbf{g}_y\|_2^2] \mathbb{E}[\mathbf{x} \mathbf{x}^\top]. \quad (19)$$

*All expectations are w.r.t. the stochasticity induced by mini-batch sampling while conditioning on the fine-tuned checkpoint.*

Assumption 1 reflects a local quasi-stationary basin in which the mean of update-drift becomes negligible and the weight norm remains stable. Condition (1) states that the averaged task-specific descent direction is balanced by the learned task vector. This resembles shrinkage around a pretrained solution in  $L_2$ -style transfer learning [23] and is consistent with terminal representation geometry, where features, weights, and gradients align along task-relevant directions [14, 17]. Condition (2) weakens exact proportionality to a cosine-similarity alignment. It allows nonzero minibatch fluctuations, but assumes that their dominant input-side second-moment geometry remains aligned with the mean task-descent geometry. This is motivated by evidence that SGD noise is anisotropic and geometry-aware rather than isotropic [24, 25]; in particular, Wu et al. [25] quantify alignment between SGD noise covariance and Fisher geometry using Frobenius-type alignment factors. Condition (3) states residual error signals become less structured, motivating a coarse decoupling between gradient energy and input activations in the spirit of K-FAC-style layer-wise curvature factorizations [26] and representation/gradient geometry views such as AGOP/NFA [15, 16].

**Theorem 1 Restated.** Under Assumption 1, the Gram matrix of input activations and the Gram matrix of task-vectors have a positively correlated alignment:

$$\cos_F\left(\mathbb{E}[\mathbf{x} \mathbf{x}^\top], (\mathbf{U}^{(t)})^\top \mathbf{U}^{(t)}\right) > \alpha_t. \quad (20)$$

*Proof.* For notational brevity, we omit the task superscript and write

$$\bar{\mathbf{D}} = \mathbb{E}[\mathbf{D}], \quad \mathbf{M} = \bar{\mathbf{D}}^\top \bar{\mathbf{D}}, \quad \mathbf{C} = \mathbb{E}[(\mathbf{D} - \bar{\mathbf{D}})^\top (\mathbf{D} - \bar{\mathbf{D}})].$$

By the second-moment decomposition,

$$\mathbb{E}[\mathbf{D}^\top \mathbf{D}] = \mathbf{M} + \mathbf{C}. \quad (21)$$

Assumption 1.1 gives

$$\mathbf{M} = \rho^2 (\mathbf{U}^{(t)})^\top \mathbf{U}^{(t)}. \quad (22)$$

Since the positive scaling by  $\rho^2$  does not affect cosine similarity, it suffices to lower-bound

$$\cos_F(\mathbf{M} + \mathbf{C}, \mathbf{M}).$$

If  $\mathbf{C} = \mathbf{0}$ , this cosine is  $1 > \alpha_t$ . Otherwise, let

$$r = \frac{\|\mathbf{C}\|_F}{\|\mathbf{M}\|_F}, \quad \gamma = \cos_F(\mathbf{C}, \mathbf{M}). \quad (23)$$

By Assumption 1.2,  $\gamma > 0$ . From the definitions of  $r$  and  $\gamma$ ,

$$\langle \mathbf{C}, \mathbf{M} \rangle_F = \gamma \|\mathbf{C}\|_F \|\mathbf{M}\|_F = r\gamma \|\mathbf{M}\|_F^2. \quad (24)$$

Moreover,

$$\|\mathbf{M} + \mathbf{C}\|_F^2 = \|\mathbf{M}\|_F^2 + \|\mathbf{C}\|_F^2 + 2\langle \mathbf{C}, \mathbf{M} \rangle_F = \|\mathbf{M}\|_F^2 (1 + r^2 + 2r\gamma). \quad (25)$$

Using Eqs. (24) and (25), the Frobenius cosine-similarity becomes

$$\begin{aligned} \cos_F(\mathbf{M} + \mathbf{C}, \mathbf{M}) &= \frac{\langle \mathbf{M} + \mathbf{C}, \mathbf{M} \rangle_F}{\|\mathbf{M} + \mathbf{C}\|_F \|\mathbf{M}\|_F} \\ &= \frac{\|\mathbf{M}\|_F^2 + \langle \mathbf{C}, \mathbf{M} \rangle_F}{\|\mathbf{M}\|_F^2 \sqrt{1 + r^2 + 2r\gamma}} = \frac{1 + r\gamma}{\sqrt{1 + r^2 + 2r\gamma}}. \end{aligned} \quad (26)$$

For  $r \geq 0$  and  $\gamma \in (0, 1]$ , we have

$$\frac{1 + r\gamma}{\sqrt{1 + r^2 + 2r\gamma}} \geq \gamma,$$

since both sides are nonnegative and the squared inequality reduces to

$$(1 - \gamma^2)(1 + 2r\gamma) \geq 0.$$

Therefore,

$$\cos_F(\mathbf{M} + \mathbf{C}, \mathbf{M}) \geq \gamma > \alpha_t. \quad (27)$$

Finally, by Eq. (21),

$$\mathbb{E}[\mathbf{D}^\top \mathbf{D}] = \mathbf{M} + \mathbf{C},$$

and by Eq. (22),

$$\mathbf{M} = \rho^2 (\mathbf{U}^{(t)})^\top \mathbf{U}^{(t)}.$$

Since  $\rho^2 > 0$ , this positive scalar does not change Frobenius cosine-similarity. Therefore Eq. (27) implies

$$\cos_F\left(\mathbb{E}[\mathbf{D}^\top \mathbf{D}], (\mathbf{U}^{(t)})^\top \mathbf{U}^{(t)}\right) > \alpha_t. \quad (28)$$

It remains to connect  $\mathbb{E}[\mathbf{D}^\top \mathbf{D}]$  to the activation Gram matrix. Since  $\mathbf{D} = \mathbf{g}_y \mathbf{x}^\top$ ,

$$\mathbf{D}^\top \mathbf{D} = \|\mathbf{g}_y\|_2^2 \mathbf{x} \mathbf{x}^\top. \quad (29)$$

Taking expectations and applying Assumption 1.3,

$$\mathbb{E}[\mathbf{D}^\top \mathbf{D}] = \mathbb{E}[\|\mathbf{g}_y\|_2^2] \mathbb{E}[\mathbf{x} \mathbf{x}^\top], \quad (30)$$

where  $\mathbb{E}[\|\mathbf{g}_y\|_2^2]$  does not change cosine similarity. Combining this with Eq. (28), we have

$$\cos_F\left(\mathbb{E}[\mathbf{x} \mathbf{x}^\top], (\mathbf{U}^{(t)})^\top \mathbf{U}^{(t)}\right) > \alpha_t. \quad (31)$$

This completes the proof. ■

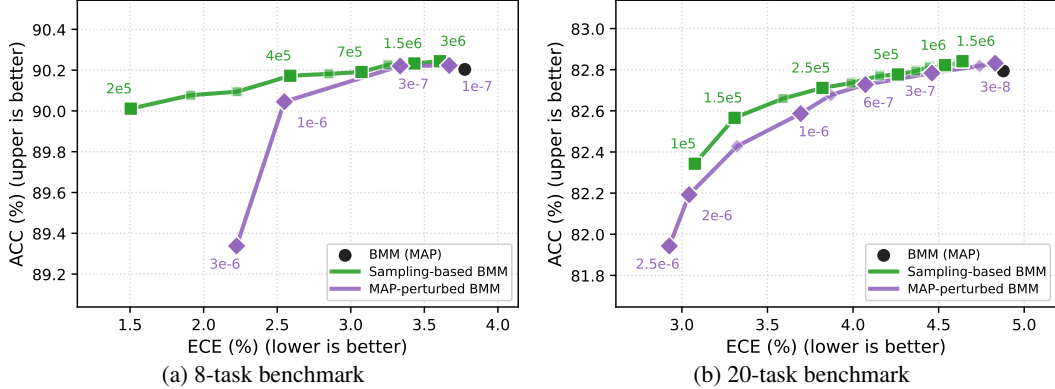


Figure 4: Pareto frontiers of sampling-based BMM vs. MAP-perturbed BMM on ViT-B/32 benchmarks. Each dot is generated by varying either  $\beta$  or  $\sigma_{iid}$ , and the black dot is the performance of BMM (MAP), corresponding to  $\beta = \infty$  or  $\sigma_{iid} = 0$ .

## B Sampling-based BMM for Uncertainty Calibration

**Sampling-based BMM.** A MAP point estimate of  $\mathbf{U}$  is used in Algorithm 1 mainly for the purpose of computational efficiency. Note that the Bayesian linear regression formulation in Sec. 4.1 leads to a Gaussian posterior  $\mathcal{N}(\mathbf{U}_{\text{MAP}}, \Sigma_{\text{row}})$  with

$$\mathbf{U}_{\text{MAP}} = \left( \mathbf{Y}\mathbf{X}^{\top} + \lambda\mathbf{U}^{(0)} \right) \left( \mathbf{X}\mathbf{X}^{\top} + \lambda\mathbf{I} \right)^{-1}, \quad \Sigma_{\text{row}} = \beta^{-1} \left( \mathbf{X}\mathbf{X}^{\top} + \lambda\mathbf{I} \right)^{-1}, \quad (32)$$

where  $\mathbf{I} \in \mathbb{R}^{d_{in} \times d_{in}}$  is the identity matrix,  $\Sigma_{\text{row}}$  is the covariance matrix for each row of  $\mathbf{U}$ , and  $\beta$  is the precision of Gaussian noise, which can be tuned on a validation set. Once  $\lambda^*$  is determined by Algorithm 1, we can sample multiple merged models for uncertainty calibration [27].

Specifically, let  $\{\theta_{\text{merged}}^{(r)}\}_{r=1}^S$  be  $S$  merged models sampled from the Gaussian posteriors (given  $\lambda^*$  and  $\beta$ ), and  $\mathbf{z}(\mathbf{x}; \theta)$  denote the logit vector of model  $\theta$ . The prediction of the model ensemble is the average probability across  $S$  merged models:

$$p(y|\mathbf{x}) = \frac{1}{S} \sum_{r=1}^S \text{softmax} \left( \mathbf{z}(\mathbf{x}; \theta_{\text{merged}}^{(r)}) \right). \quad (33)$$

As we will see, this model ensemble improves the uncertainty calibration as measured by ECE, a standard metric for this purpose.

**Expected Calibration Error.** ECE is a commonly adopted metric to measure the calibration of a model. First, it computes the confidence of the model,  $\max_y p(y|\mathbf{x}_i)$ , for each  $\mathbf{x}_i$  in the dataset. Then it groups the predictions into equally spaced buckets  $\{B_1, B_2, \dots, B_{\kappa}\}$  based on their confidence scores. For example, if  $\kappa = 20$ , then  $B_1$  would represent all examples for which the model’s confidence scores were between 0 and 0.05. Then ECE is calculated as

$$\text{ECE} = \sum_{b=1}^{\kappa} \frac{|B_b|}{n} |\text{acc}(B_b) - \text{conf}(B_b)|, \quad (34)$$

where  $n$  is the number of examples in the dataset,  $\text{acc}(B_b)$  is the average accuracy of the model on all the examples in  $B_b$  and  $\text{conf}(B_b)$  is the average confidence on all the examples in  $B_b$ . In our experiments, we set  $\kappa = 20$ . For a perfectly calibrated model, the ECE will be 0 for any  $\kappa$ .

**Experimental Setup.** We evaluate the uncertainty calibration of model ensemble, constructed from sampling-based BMM (controlled by  $\beta$ ), on the ViT-B/32 8-task and 20-task benchmarks in the data-assisted setting, where ISO-CTS serves as the anchor model. Preliminary experiments show that sampling only for the last MLP output matrix leads to the most prominent ECE performance – similar observations have also been made by [28]. As a baseline, we also perturb the MAP solution of the last MLP output matrix with IID Gaussian noise (controlled by  $\sigma_{iid}$ ). Both methods generate  $S = 10$  samples of merged models, and use the average prediction of Eq. 33 for final classification. By varying  $\beta$  and  $\sigma_{iid}$ , each model ensemble trades-off between classification accuracies and ECE scores, and the Pareto frontiers of both methods are reported in Figure 4.

**Results and Analysis.** As can be seen, the Pareto frontier of sampling-based BMM dominates that of MAP-perturbed BMM, indicating a better trade-off between classification accuracies and ECE scores for the former. In addition, the gap between two Pareto frontiers is more pronounced on the 8-task benchmark, indicating that merging on 20-task benchmark is more challenging and the flexibility for the tradeoff is limited.

## C Experimental Protocol and Assets

### C.1 Vision Benchmarks

For the *vision* experiments, to ensure a rigorous and fair comparison, we strictly adhere to the benchmarks established by TSV [8] and ISO-CTS [9], adopting their exact datasets and identical training, validation, and test splits. Specifically, our evaluation spans three benchmarks with increasing task diversity. The initial 8-task benchmark comprises Stanford Cars [29], DTD [30], EuroSAT [31], GTSRB [32], MNIST [33], RESISC45 [34], SUN397 [35], and SVHN [36]. The 14-task benchmark extends this setting by adding CIFAR-100 [37], STL-10 [38], Flowers102 [39], Oxford-IIIT Pets [40], PCAM [41], and FER2013 [42]. Finally, the largest benchmark encompasses 20 tasks by further incorporating EMNIST [43], CIFAR-10 [37], Food101 [44], Fashion-MNIST [45], Rendered SST-2 [46], and KMNIST [47]. Table 1 in the main paper reports the performance of the merged models averaged across the 8, 14, and 20 tasks, while the “mean  $\pm$  std” results and the per-task breakdown radar charts are provided in Appendices E.1 and E.2, respectively.

### C.2 Language Benchmarks

Table 4: Summary of training and evaluation datasets for natural language processing experiments. Official standard splits are adopted for all benchmarks, with the exception of the GSM8k validation set (500 samples from the training set) and datasets marked with \* (custom 1/3-2/3 splits).

Category	Training	Validation	Test	Metric
Instruction	TULU-3 Persona [48]	IFEval* [49]	IFEval* [49]	Prompt Acc.
Mathematics	DART [50], Nu- minaMath [51]	GSM8k [52]	GSM8k [52]	EM (8-shot)
Multilingual	Aya [53]	M_MMLU [54] (fr, es, de, ru)	M_MMLU [54] (fr, es, de, ru)	Accuracy
Coding	Magicoder [55]	MBPP [56]	HumanEval+ [57], MBPP+ [57]	Pass@1
Safety	WildGuard [58], WildJail- break [59]	HarmBench* [60], XSTest* [61]	HarmBench* [60], XSTest* [61]	RTA / Acc.

For the NLP experiments, Table 4 summarizes the training, validation, and test splits, together with the corresponding evaluation metrics. Our evaluation covers five task categories. For categories involving multiple test sets, we first average the individual test scores within each category to obtain a category-level score. Throughout the main text, we report the macro-average over the five category-level scores as the overall performance, while category-level language breakdowns are provided in Appendix E.2.

### C.3 Licenses and Asset Usage

We use existing public assets, including pretrained backbones, task-specific checkpoints, benchmark datasets, evaluation suites, and baseline implementations. These assets are described above, and their original creators are credited through the corresponding references.

For vision experiments, we follow public model-merging benchmark settings based on ViT backbones and task-specific expert checkpoints. For language experiments, we use Llama-3.2-3B and Llama-3.1-8B backbones under the corresponding Meta Llama Community License Agreements and acceptable-

use policy. We do not redistribute third-party checkpoints or model weights except where permitted by their original licenses.

All datasets and evaluation suites are used only for research, calibration, validation, and evaluation. Their source URLs, versions when applicable, and license or source-term information are provided in the supplementary asset manifest. Safety benchmarks may contain harmful or adversarial prompts and are used only for safety research and evaluation.

Baseline methods and third-party libraries are used according to their original papers, public repositories, and licenses. We retain required copyright notices, citations, and license files where applicable. We do not introduce new scraped datasets or human-subject data. All copyrights remain with the original asset owners, and all external assets are used in compliance with their respective licenses and terms of use.

## D Computational Costs and Runtime

### D.1 Complexity Analysis

We briefly analyze the costs of the closed-form estimators (Eqs. 8, 15) and the BO search (12). Let  $T$  be the number of tasks,  $M$  be the number of merged 2D modules, and  $\mathbf{U}_m \in \mathbb{R}^{d_{\text{out},m} \times d_{\text{in},m}}$ . In the data-assisted setting, with  $N$  calibration samples per task,  $\mathbf{X}_m \in \mathbb{R}^{d_{\text{in},m} \times N_{\text{act}}}$  and  $\mathbf{Y}_m \in \mathbb{R}^{d_{\text{out},m} \times N_{\text{act}}}$ , where  $N_{\text{act}} = NT$ . We omit the one-time forward cost for collecting activations.

**Closed-form estimators.** The data-assisted estimator in Eq. (8) first caches  $\mathbf{X}_m \mathbf{X}_m^\top$  and  $\mathbf{Y}_m \mathbf{X}_m^\top$ , which costs  $\mathcal{O}(N_{\text{act}} d_{\text{in},m}^2 + N_{\text{act}} d_{\text{out},m} d_{\text{in},m})$ . Then, given a module-wise  $\lambda_m$ , solving

$$(\mathbf{X}_m \mathbf{X}_m^\top + \lambda_m \mathbf{I}) \mathbf{U}_m^\top = (\mathbf{Y}_m \mathbf{X}_m^\top + \lambda_m \mathbf{U}_m^{(0)})^\top,$$

costs  $\mathcal{O}(d_{\text{in},m}^3 + d_{\text{out},m} d_{\text{in},m}^2)$  by using a dense Cholesky solver [62]. Therefore, assuming a square 2D module for simplicity, the total cost is  $\mathcal{O}(d^3)$ . Similarly, the data-free estimator in Eq. (15) replaces activation statistics with the Gram-matrix of task vectors, whose construction costs  $\mathcal{O}(T d_{\text{out},m} d_{\text{in},m}^2)$  per module, followed by the same Cholesky solver, and leads to the same total cost of  $\mathcal{O}(d^3)$ . Typically,  $d = 1,024$  in our benchmarks. Thus, the cost of the closed-form estimators is insignificant on modern high-performance GPUs.

**BO search overhead.** Algorithm 1 performs  $K$  BO trials. The exact  $\mathcal{GP}$  update costs  $\mathcal{O}(K^3)$  due to the Cholesky factorization of the  $\mathcal{GP}$  kernel matrix [21, 63]. In practice, this overhead is very small compared with repeated validation-set evaluations. Hence, the practical runtime of BO is dominated by evaluating candidate merged models on the validation set.

### D.2 Runtime Breakdown

Table 5 reports the wall-clock runtime of the BMM pipeline. The vision experiments with  $K = 200$  BO trials are measured on a single NVIDIA RTX A6000 48GB, with validation tensors cached locally to reduce I/O overhead. The language experiments with  $K = 100$  BO trials report per-worker timings under an 8-GPU parallel setup. Across both vision and language benchmarks, the algorithmic overhead of BMM remains small compared with validation-set forward passes, indicating that the main runtime cost comes from model evaluation rather than from the BMM update itself.

### D.3 Runtime–Performance Trade-offs

As shown in Figure 3 (right) and Table 6, BMM provides favorable runtime–performance trade-offs in the data-free setting, even under constrained BO budgets. On the 20-task ViT-B/32 benchmark, BMM with only  $K = 20$  trials outperforms all grid-search anchors while requiring substantially less wall-clock time. Increasing the budget to  $K = 60$  further improves the score to 81.52%. This efficiency stems from BMM’s closed-form updates and BO-based search, which avoid the main bottlenecks of baseline methods: WUDI-Merging relies on costly iterative SGD optimization, whereas ISO-CTS requires exhaustive grid search over 225 configurations. For Llama-3.2-3B, BMM also substantially reduces search cost. With  $K = 20$ , it reaches a score close to the strongest TSV baseline in less

Table 5: **Runtime breakdown of BMM on vision and language tasks.** The ViT timings are measured on a single NVIDIA A6000 GPU, while the Llama timings are reported per worker under an 8-way parallel BO execution. *Gram* denotes the one-time Gram-matrix construction cost in the data-assisted setting. *Closed-form* and *GP* denote the cumulative costs of closed-form solution and GP surrogate updates, respectively. *Search* includes Gram construction, closed-form solution, GP updates, model assembly, checkpoint loading/book-keeping, and rounding. *Val. Cost* reports the time spent on validation-set evaluations.

Model	Tasks	Setting	Gram	Closed-form	GP	Search	Val. Cost	Total
ViT-B/32	8	data-assisted	0.4 min	2.5 min	0.4 min	3.3 min	17.3 min	20.6 min
ViT-B/32	8	data-free	–	2.2 min	0.4 min	2.9 min	17.3 min	20.2 min
ViT-B/32	14	data-assisted	0.6 min	4.5 min	0.4 min	6.2 min	22.3 min	28.5 min
ViT-B/32	14	data-free	–	5.2 min	0.4 min	5.6 min	22.3 min	27.9 min
ViT-B/32	20	data-assisted	0.8 min	4.6 min	0.4 min	8.0 min	41.6 min	49.6 min
ViT-B/32	20	data-free	–	6.9 min	0.4 min	7.3 min	41.6 min	48.8 min
ViT-L/14	8	data-assisted	2.8 min	8.2 min	0.4 min	17.1 min	168.4 min	185.5 min
ViT-L/14	8	data-free	–	13.9 min	0.4 min	14.3 min	168.4 min	182.7 min
ViT-L/14	14	data-assisted	5.8 min	12.1 min	0.4 min	18.6 min	292.1 min	310.7 min
ViT-L/14	14	data-free	–	11.3 min	0.4 min	12.8 min	292.1 min	304.9 min
ViT-L/14	20	data-assisted	9.8 min	17.0 min	0.4 min	31.7 min	539.0 min	570.7 min
ViT-L/14	20	data-free	–	21.5 min	0.4 min	21.9 min	539.0 min	560.9 min
Llama-3.2-3B	5	data-assisted	1.0 min	12.9 min	0.1 min	14.5 min	126.9 min	141.4 min
Llama-3.2-3B	5	data-free	–	13.4 min	0.1 min	13.5 min	126.9 min	140.3 min
Llama-3.1-8B	5	data-assisted	2.8 min	38.4 min	0.1 min	43.4 min	190.7 min	234.1 min
Llama-3.1-8B	5	data-free	–	39.9 min	0.1 min	39.9 min	190.7 min	230.6 min

Table 6: Runtime and performance comparison of BMM and state-of-the-art data-free merging methods. For ViT-B/32, BMM uses ISO-CTS as anchor; for Llama-3.2-3B, BMM uses TSV as anchor. Baselines use their full grid-search budgets, whereas BMM is evaluated with BO budgets of  $K = 20$  and  $K = 60$ . The ViT runtimes are measured on a single NVIDIA A6000 GPU, and the Llama runtimes report 8-GPU parallel wall-clock time. Scores denote test accuracies for ViT-B/32 and aggregate benchmark scores for Llama-3.2-3B.

Model	Tasks	Method	Search Dim.	#Trials	Runtime	Score
ViT-B/32	20	TSV	1	30	8.4 min	76.9
ViT-B/32	20	WUDI-Merging	2	24	116.1 min	76.1
ViT-B/32	20	ISO-CTS	3	225	91.2 min	77.6
ViT-B/32	20	BMM ( $K = 20$ )	15	20	5.60 min	80.0
ViT-B/32	20	BMM ( $K = 60$ )	15	60	15.55 min	81.5
Llama-3.2-3B	5	TSV	1	30	73.4 min	0.471
Llama-3.2-3B	5	WUDI-Merging	2	24	418.8 min	0.461
Llama-3.2-3B	5	ISO-CTS	3	225	318.0 min	0.441
Llama-3.2-3B	5	BMM ( $K = 20$ )	5	20	28.6 min	0.465
Llama-3.2-3B	5	BMM ( $K = 60$ )	5	60	84.8 min	0.473

than half of TSV’s wall-clock time and far less time than WUDI-Merging or ISO-CTS. These results suggest that BMM’s closed-form solution combined with BO-based search provides an efficient model merging method across both vision and language benchmarks.

## E Additional Experimental Results

### E.1 Detailed results on vision tasks with standard deviations

Table 7 provides the comprehensive results corresponding to Table 1, including standard deviations across five random seeds (0–4). The results demonstrate minimal variance across all settings, with standard deviations predominantly ranging from  $\pm 0.01$  to  $\pm 0.06$ . The low variance confirms that the performance improvements achieved by BMM are stable and robust, rather than artifacts of specific seed initializations.

Table 7: Model merging on vision tasks with ViT architectures. Values represent the mean accuracy over five independent runs (seeds 0–4). Black subscripts indicate the standard deviation, which are omitted in Table 1 due to lack of space. (Indiv.: Individual)

Model	Tasks	Setting	Indiv.	Pretrained	TA	TIES	RegMean	TSV	WUDI	ISO-CTS
ViT-B/32	8	anchor	92.8	47.7	70.4	75.7	82.3	85.9	<b>87.0</b>	86.4
		data-assisted	-	84.8 $\pm$ 0.02	85.0 $\pm$ 0.05	85.7 $\pm$ 0.03	85.2 $\pm$ 0.05	88.9 $\pm$ 0.05	89.4 $\pm$ 0.02	<b>90.2</b> $\pm$ 0.03
		data-free	-	87.9 $\pm$ 0.06	87.0 $\pm$ 0.05	87.0 $\pm$ 0.06	87.9 $\pm$ 0.09	87.8 $\pm$ 0.04	87.6 $\pm$ 0.04	<b>89.0</b> $\pm$ 0.03
	14	anchor	90.9	56.9	65.2	68.2	76.6	79.9	80.5	<b>81.5</b>
		data-assisted	-	78.9 $\pm$ 0.03	79.2 $\pm$ 0.04	79.7 $\pm$ 0.04	79.1 $\pm$ 0.02	84.3 $\pm$ 0.04	84.6 $\pm$ 0.04	<b>85.5</b> $\pm$ 0.06
		data-free	-	82.7 $\pm$ 0.06	82.4 $\pm$ 0.03	82.3 $\pm$ 0.10	82.9 $\pm$ 0.09	82.8 $\pm$ 0.03	81.7 $\pm$ 0.06	<b>84.3</b> $\pm$ 0.05
	20	anchor	91.3	55.7	60.4	64.0	72.2	76.9	76.1	<b>77.6</b>
		data-assisted	-	75.6 $\pm$ 0.05	75.5 $\pm$ 0.04	76.3 $\pm$ 0.03	75.9 $\pm$ 0.06	82.0 $\pm$ 0.04	82.2 $\pm$ 0.06	<b>82.8</b> $\pm$ 0.05
		data-free	-	80.0 $\pm$ 0.06	78.4 $\pm$ 0.06	79.2 $\pm$ 0.05	79.7 $\pm$ 0.03	79.7 $\pm$ 0.05	78.0 $\pm$ 0.02	<b>81.5</b> $\pm$ 0.04
ViT-L/14	8	anchor	95.8	65.1	84.8	87.0	90.0	93.0	94.0	<b>94.8</b>
		data-assisted	-	92.3 $\pm$ 0.01	92.8 $\pm$ 0.05	93.1 $\pm$ 0.03	92.7 $\pm$ 0.03	94.4 $\pm$ 0.03	94.7 $\pm$ 0.02	<b>95.1</b> $\pm$ 0.03
		data-free	-	94.4 $\pm$ 0.02	94.2 $\pm$ 0.01	94.2 $\pm$ 0.03	94.0 $\pm$ 0.02	94.4 $\pm$ 0.01	94.3 $\pm$ 0.04	<b>95.0</b> $\pm$ 0.02
	14	anchor	94.3	68.5	79.4	80.2	85.5	89.1	90.5	<b>91.0</b>
		data-assisted	-	88.0 $\pm$ 0.01	88.3 $\pm$ 0.03	88.3 $\pm$ 0.03	88.2 $\pm$ 0.02	91.6 $\pm$ 0.01	91.7 $\pm$ 0.03	<b>92.2</b> $\pm$ 0.07
		data-free	-	90.9 $\pm$ 0.08	90.9 $\pm$ 0.04	90.8 $\pm$ 0.02	90.6 $\pm$ 0.05	91.3 $\pm$ 0.05	91.0 $\pm$ 0.06	<b>92.1</b> $\pm$ 0.06
	20	anchor	94.7	65.4	74.0	76.7	82.8	87.7	88.4	<b>90.1</b>
		data-assisted	-	86.0 $\pm$ 0.02	86.2 $\pm$ 0.03	86.4 $\pm$ 0.01	86.2 $\pm$ 0.01	90.9 $\pm$ 0.03	90.8 $\pm$ 0.02	<b>91.5</b> $\pm$ 0.01
		data-free	-	89.8 $\pm$ 0.02	89.6 $\pm$ 0.01	89.5 $\pm$ 0.01	89.4 $\pm$ 0.04	90.3 $\pm$ 0.02	89.7 $\pm$ 0.02	<b>91.1</b> $\pm$ 0.11

## E.2 Radar Charts: Per-Task Breakdowns

Tables 1 and 2 report the performance of merged models averaged across multiple tasks. However, such summaries may hide task-specific trade-offs. To address this issue, Figures 5–8 provide vision per-task radar charts for all evaluated ViT settings. Similarly, Figures 9–10 provide language per-task radar charts for all evaluated Llama settings.

**Key Observations.** In most evaluated settings, BMM exhibits a Pareto dominance over the corresponding anchor baselines, improving every task without reducing performance on any individual task. This indicates that the average gains reported in Tables 1 and 2 generally reflect a broad multi-task expansion rather than a redistribution of performance across tasks. The strong overlap between the data-assisted and data-free curves further suggests that our data-free surrogate captures much of the task geometry revealed by the calibration-based estimate, enabling competitive data-free model merging without any auxiliary calibration data.







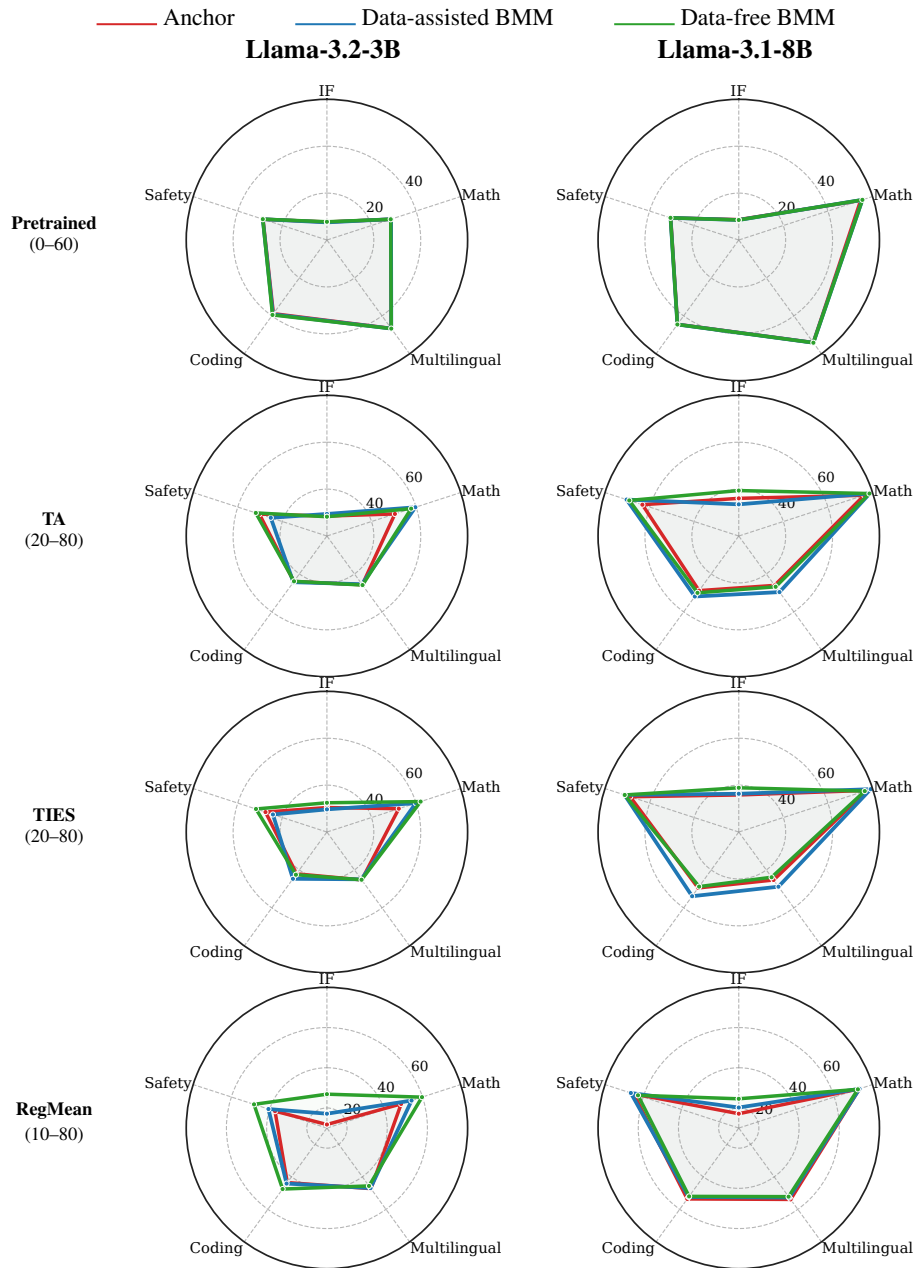


Figure 9: **Radar charts: Llama per-task breakdowns** (corresponding to Table 2). The radial axis limits (min-max) are annotated on the left. “IF” denotes Instruction Following.

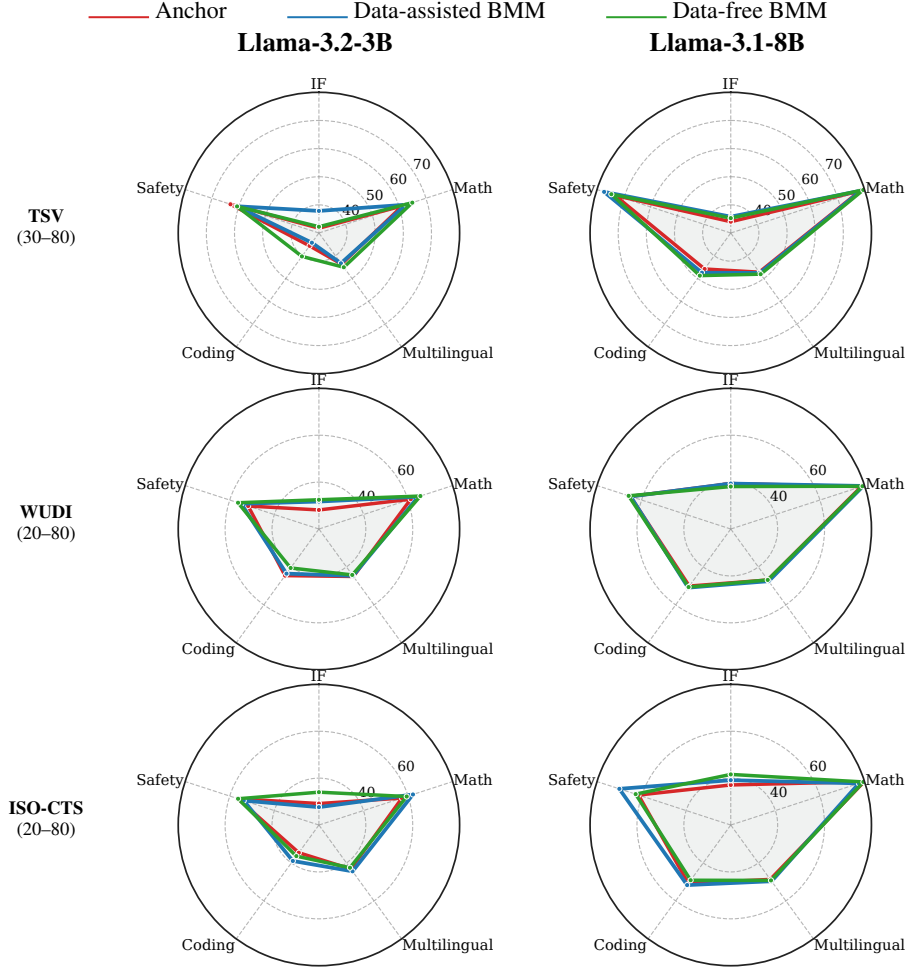


Figure 10: **Radar charts: Llama per-task breakdowns** (corresponding to Table 2). Continued from Figure 9 on the remaining anchor models. “IF” denotes Instruction Following.

## F A Hybrid Estimate of Gram Matrix in Few-Shot Regimes

Theorem 1 indicates that the Gram matrix  $\mathbb{E}[\mathbf{x}\mathbf{x}^\top]$  can be estimated empirically from few-shot calibration samples (data-assisted) or approximated by the expert-weight surrogate  $\mathbf{U}^\top \mathbf{U}$  (data-free). Therefore, a hybrid estimate of Gram matrix may be worthy of investigation. We consider a *mix* variant that interpolates between the few-shot empirical estimate and the data-free surrogate:

$$\mathbf{G}_m^{\text{mix}}(\epsilon) = \epsilon \mathbf{G}_m^{\text{few}} + (1 - \epsilon) \mathbf{G}_m^{\text{df}}, \quad \epsilon \in [0, 1], \quad (35)$$

where  $\mathbf{G}_m^{\text{few}} = \mathbf{X}_m \mathbf{X}_m^\top$  is estimated from few-shot calibration samples,  $\mathbf{G}_m^{\text{df}} = \sum_{t=1}^T (\mathbf{U}_m^{(t)})^\top \mathbf{U}_m^{(t)}$  is the data-free estimate, and the mixing weight  $\epsilon$  is optimized by BO.

Table 8 shows this *mix* variant consistently improves upon the pure data-free variant and often enhances few-shot results, particularly for TSV and ISO-CTS. This is likely because the 1-shot or 5-shot empirical estimates are often noisy and rank-deficient, and the data-free surrogate provides a reliable estimate based on the weights of expert models. As can be seen, *1-shot mix* boosts 8-task TSV accuracy from 87.8% to 88.9%, and *5-shot mix* improves 20-task ISO-CTS from 82.2% to 83.7%. Although the *mix* variant is very close to pure few-shot estimates for WUDI in certain cases, its overall robustness confirms that blending limited empirical statistics with data-free surrogate is highly effective in few-shot regimes.

Table 8: Different Gram matrix estimation strategies and their impacts on 8-, 14-, and 20-task merging with ViT-B/32 architecture. The *mix* variant interpolates between data-assisted Gram matrix estimate (1-shot or 5-shot) and data-free estimate by a BO-optimized weight. Results for data-free and data-assisted variants are reported as mean  $\pm$  std over seeds 0–4.

Setting	8 Tasks			14 Tasks			20 Tasks		
	TSV	WUDI	ISO-CTS	TSV	WUDI	ISO-CTS	TSV	WUDI	ISO-CTS
anchor	85.9	87.0	86.4	79.9	80.5	81.5	76.9	76.1	77.6
data-free	87.8 $\pm$ 0.04	87.6 $\pm$ 0.04	89.0 $\pm$ 0.03	82.8 $\pm$ 0.03	81.7 $\pm$ 0.06	84.3 $\pm$ 0.05	79.7 $\pm$ 0.05	78.0 $\pm$ 0.02	81.5 $\pm$ 0.04
1-shot	87.8 $\pm$ 0.06	<b>89.0<math>\pm</math>0.02</b>	88.7 $\pm$ 0.03	83.2 $\pm$ 0.15	<b>84.1<math>\pm</math>0.06</b>	84.2 $\pm$ 0.07	80.6 $\pm$ 0.06	<b>81.1<math>\pm</math>0.04</b>	80.5 $\pm$ 0.06
1-shot mix	<b>88.9<math>\pm</math>0.05</b>	<b>89.0<math>\pm</math>0.08</b>	<b>89.7<math>\pm</math>0.05</b>	<b>84.3<math>\pm</math>0.07</b>	<b>84.1<math>\pm</math>0.05</b>	<b>85.7<math>\pm</math>0.04</b>	<b>81.5<math>\pm</math>0.15</b>	<b>81.1<math>\pm</math>0.03</b>	<b>82.8<math>\pm</math>0.03</b>
5-shot	88.5 $\pm$ 0.11	<b>89.3<math>\pm</math>0.06</b>	89.5 $\pm$ 0.03	84.1 $\pm$ 0.04	<b>84.6<math>\pm</math>0.07</b>	85.3 $\pm$ 0.04	81.7 $\pm$ 0.02	<b>81.9<math>\pm</math>0.04</b>	82.2 $\pm$ 0.02
5-shot mix	<b>89.4<math>\pm</math>0.11</b>	<b>89.3<math>\pm</math>0.07</b>	<b>90.2<math>\pm</math>0.02</b>	<b>84.9<math>\pm</math>0.11</b>	<b>84.6<math>\pm</math>0.08</b>	<b>86.1<math>\pm</math>0.06</b>	<b>82.4<math>\pm</math>0.03</b>	<b>81.9<math>\pm</math>0.03</b>	<b>83.7<math>\pm</math>0.02</b>